Necrosis-induced apoptosis promotes regeneration in *Drosophila* wing imaginal discs

Jacob Klemm, Michael J. Stinchfield, Robin E. Harris

School of Life Sciences, Arizona State University, Tempe, AZ 85287-4501

Running Title: Necrosis-induced wing disc regeneration

Keywords: regeneration, cell death**,** Drosophila, apoptosis, gene expression, necrosis, imaginal disc

Corresponding Author Details:

Robin Harris,

Arizona State University

427 E Tyler Mall LSE 229

Attn: Dr. Rob Harris, LSE 333

Tempe

AZ 85287-4501

Robin.Harris@ASU.edu

(480)965 7543

Abstract

Regeneration is a complex process that requires a coordinated genetic response to tissue loss. Signals from dying cells are crucial to this process and are best understood in the context of regeneration following programmed cell death, like apoptosis. Conversely, regeneration following unregulated forms of death such as necrosis have yet to be fully explored. Here we have developed a novel method to investigate regeneration following necrosis using the *Drosophila* wing imaginal disc. We show that necrosis stimulates regeneration at levels comparable to that of apoptosis-mediated cell death, and activates a similar response at the wound edge involving local JNK signaling. Unexpectedly however, necrosis also results in significant apoptosis far from the site of ablation, which we have termed necrosis-induced apoptosis (NiA). This apoptosis occurs independent of changes at the wound edge and importantly does not rely on JNK signaling. Furthermore, we find that blocking NiA inhibits blastema formation and subsequently limits regeneration, suggesting that tissues damaged by necrosis activate programmed cell death at a distance from the injury to promote regeneration.

Introduction

Apoptosis has a fundamental role in shaping organisms during development and in maintaining tissue homeostasis (Fuchs and Steller 2011; Suzanne and Steller 2013). This vital cellular process acts to counter infection, suppress tumor formation and promote recovery from damage (Fogarty and Bergmann 2017; Hacker 2018; Wong 2011). These events can occur because dying cells release signals that act on surrounding cells, leading to different cellular outcomes depending on the context and on the nature of the signal (Fogarty and Bergmann 2015; Fuchs and Steller 2015; Perez-Garijo and Steller 2015; Su 2015). Successful regeneration following injury can also depend on this apoptotic signaling, which has been shown to regulate various aspects of recovery including morphogenesis, inflammation and tissue regrowth (Bergmann and Steller 2010; Perez-Garijo and Steller 2015; Vriz et al. 2014). In many organisms, factors released from dying cells stimulate the proliferation of adjacent cells as a replacement mechanism (Chera et al. 2009; Li et al. 2010; Pellettieri et al. 2010; Su 2015; Tseng et al. 2007; Vriz et al. 2014). This specialized form of compensatory proliferation is known as apoptosis-induced proliferation (AiP) (Fogarty and Bergmann 2017), in which a number of mitogens, including WNTs, TGFβ, EGF and Hedgehog, are released from dying cells as part of this mechanism (Fogarty and Bergmann 2017; Fuchs and Steller 2015). Upstream factors that lead to their production, such as JNK signaling and the activation of caspases, have also been described (Fogarty and Bergmann 2017; Pinal et al. 2019). Conversely, apoptosis can also promote the death of surrounding cells, a process known as apoptosis-induced apoptosis (AiA), (Fogarty and Bergmann 2015; Perez-Garijo et al. 2013; Su 2015). This process also relies on JNK signaling and possibly represents a

58 mechanism to ensure the proper coordination of cell death (Perez-Garijo et al. 2013).
59 Signals from dying cells can also result in non-autonomous protection from cell death,
60 ensuring the preservation of neighboring cells after injury (Bilak et al. 2014). Thus, cell
61 death can strongly influence the behavior of surrounding cells and consequently regulate
62 the ability of a tissue to recover from damage.
63
64 Evidence that signals from apoptotic cells impact surrounding tissues first originated from
65 studies of the *Drosophila* wing imaginal disc, a larval epithelial tissue that forms the adult
66 wing (Huh et al. 2004; Perez-Garijo et al. 2004; Ryoo et al. 2004). The wing disc has been
67 extensively characterized as a model for growth and development, and for its significant
68 capacity to regenerate (Beira and Paro 2016; Hariharan and Serras 2017; Worley et al.
69 2012). Much of our understanding of imaginal disc regeneration has been through the
70 use of GAL4/UAS-based genetic ablation tools, in which tissue-specific apoptosis is
71 induced by a temperature change, permitting the study of regeneration *in situ* (Fox et al.
72 2020). However, these ablation tools rely on activating the apoptotic machinery to induce
73 damage, limiting our ability to explore other types of cell death. One such example is
74 necrosis, the rapid and disordered death of a cell characterized by the loss of membrane
75 integrity and release of cytoplasmic contents into the surrounding tissue (Fuchs and
76 Steller 2015). A number of factors released by cells undergoing necrosis have been
77 identified and characterized as signaling molecules that might influence the behavior of
78 surviving tissues, although their role in wound recovery and regeneration is not well
79 understood. In humans, necrosis can occur in all types of tissues and results from
80 environmental insults like burns or frostbite, microbial infection (Bonne and Kadri 2017;

81 Hakkarainen et al. 2014), and from common ischemic events such as heart attacks and
82 strokes (Konstantinidis et al. 2012; Radak et al. 2017; Yuan 2009). Various inherited and
83 congenital conditions can also lead to necrosis, including joint disorders and sickle cell
84 anemia (Masi et al. 2007; Milner et al. 1991). Thus, a better understanding of how a tissue
85 responds to damage could advance therapeutic methods to improve healing and
86 regeneration in a large number of human disease and injury contexts.
87
88 Here we have developed a method to induce necrotic cell death in the wing imaginal disc
89 and used it to characterize the genetic response to necrosis compared to apoptosis. Our
90 results show that wing discs can regenerate following necrosis but do so by inducing
91 extensive JNK-independent apoptosis at a distance from the site of injury. Importantly,
92 we demonstrate that this necrosis-induced apoptosis is required for proper blastema
93 formation and efficient regeneration.

Materials and Methods

Drosophila stocks and crosses

Flies were cultured in conventional dextrose fly media at 25ºC at 12 hr light-dark cycles. The recipe for dextrose media contains 9.3 g agar, 32 g yeast, 61 g cornmeal, 129 g dextrose, and 14 g tego in 1 L distilled water. Complete fly line details and RRIDs are available in the Reagent Table. The lines used as ablation stocks are as follows: *hsflp; hsp65; R85E08-DBD, DVE>>Gal4* (*DC^{NA}), hsflp; lexAop-GluR1^{Lc}, hsp65; R85E08-DBD, DVE>Gal4/S-T* (*DC^{GluR1}), hsflp; lexAOp-GluR1^{Lc}, hsp65/CyO; R85E08-DBD/TM6C, sb* (*DC^{GLuR1} no Gal4*), *hsflp; lexAop-hep^{CA}, hsp65; R85E08-DBD, DVE>>Gal4/S-T* (*DC^{hepCA}*), and *hsflp; lexaOp-rpr, hsp65/CyO, R85E08-DBD, DVE>>Gal4* (*DC^{rpr},* Harris et al., 2020). The following stock was generated for this study: *UAS-miRHG; PCNA-GFP*. The stock *DR^{wnt}* was used as a marker for early regeneration (Harris et al., 2016). The following stocks were obtained from Bloomington Drosophila Stock Center: *UAS-y^{RNAi}* (64527), *UAS-p35* (5073), *PCNA-GFP* (25749), *UAS-bsk^{RNAi}* (53310), *UAS-bsk^{DN}* (9311), *UAS-egr^{RNAi}* (58993), *puc^{A251}* (11173), *hep^{r75}* (6761), *UAS-hepCA* (58981), *nos-PhiC31:int; su(Hw)attP5* (32231). *CyclinE-disc-GFP* was a gift from the Wei Du lab. *UAS-grnd^{RNAi}* was a gift from the Bilder lab at UC Berkeley. *UAS-miRHG* and *UAS-nlsGFP; egr-Gal4* were gifts from the Hariharan lab at UC Berkeley. *UAS-GluR1^{Lc8}* (Liu et al. 2014) was obtained from the Xie lab at Stowers Institute.

Generation of *lexAOp-hep^{CA}* and *lexAOp-GluR1^{LC}* flies

To generate *lexAop-hep^{CA}*, the coding region for *hep^{CA}* was cloned from *UAS-hep^{CA}* stock and subcloned into the *lexAop-GFP* vector following excision of GFP, using XhoI and XbaI

117 sites. *LexAop-GluR1*^{LC} was generated by cloning out the *GluR1*^{LC} coding region from
118 *UAS-GluR1*^{Lc8} and subcloning it into the *lexAop-GFP* vector following excision of the GFP,
119 using XhoI and XbaI sites. The *lexAop-hep*^{CA} and *lexAop-GluR1*^{LC} constructs were
120 sequence verified and inserted into the Su(Hw)attP5 landing site via PhiC31 insertion.
121 Transgenic flies were generated by embryo injections performed by BestGene, Inc.
122

123 **Ablation Experiments**

124 DUAL Control experiments were performed essentially as described by Harris et al. 2020.
125 Experimental crosses were cultured at 25ºC and density controlled at 50 larvae per vial.
126 Larvae were ablated at day 3.5 or 4.5 of development (84 and 108 hours after egg lay
127 (AEL), respectively) by placing vials in a 37ºC water bath for 45 minutes followed by a
128 return to 25ºC. The non-ablating version of DUAL Control (DC^{NA}) was used as a control
129 while *UAS-y*^{RNAi} was used as a control for RNAi experiments. Unless stated otherwise,
130 all wing disc images taken were from larvae ablated on day 3.5 that had recovered for 18
131 hours.
132

133 **Regeneration Scoring and Wing Measurements**

134 For each experiment two sets of larvae were heat shocked, one at day 3.5 and one at
135 day 4.5 of development, reflecting times of high and low regenerative capacity,
136 respectively. Larvae were left to pupariate into adults, whose wings were scored and
137 measured. The left wing of each adult fly was used for binning into categories for
138 regeneration scoring. For measurements wings were mounted in Permount solution and
139 photographed using a Zeiss Discovery.V8 microscope and measured using the Image J

140 software. Male and female adults were measured separately, to account for sex
141 differences in wing size, using a reproducible measuring protocol that excludes the
142 variable hinge region of the wing (details of measuring protocol available on request).
143 Statistics were performed using GraphPad Prism 9.0.
144
145 **Immunohistochemistry**
146 Unless otherwise noted, early L3 larvae were dissected 18 hours after the heat shock,
147 while regeneration was still ongoing. Larvae were dissected in PBS followed by a 20-
148 minute fix in 4% paraformaldehyde in PBS. After 3 washes in 0.1% PBST (Triton-X),
149 larvae were washed in 0.3% PBST and then blocked in 0.1% PBST with 5% NGS for 30
150 minutes. Primary staining was done overnight at 4°C, while secondary staining was done
151 for 4 hours at room temperature. The following primary antibodies were obtained from the
152 Developmental Studies Hybridoma Bank: mouse anti-Nubbin (1:25), mouse anti-Wg
153 (1:100), Mouse anti-Mmp1 C-terminus (1:100), Mouse anti-Mmp1 catalytic domain
154 (1:100), mouse anti-LacZ (1:100), and rat anti-DE-Cahdherin (1:100). Rabbit anti-Dcp1
155 (1:1000) was obtained from Cell Signaling Technologies, and chick anti-GFP (1:2000)
156 was obtained from Abcam. The secondary anti-Chick 488 antibody was obtained from
157 Abcam as well. Other secondary antibodies, anti-rabbit 647, anti-rat 647, and anti-mouse
158 555 were obtained from Invitrogen. All secondary fluorophore-conjugated antibodies were
159 used at 1:500. Images were obtained on a Zeiss AxioImager.M2 with ApoTome. For each
160 experiment at least 15 discs were analyzed prior to choosing a representative image.
161 Images were processed using Affinity Photo and Affinity Designer.
162

163 **Propidium Iodide staining and TUNEL Assay**

164 Propidium iodide (PI) staining was achieved by incubating freshly dissected wing imaginal
165 discs in Schneider's Media with 15μM PI for 10 minutes, followed by several washes in
166 PBS and immediately mounting and imaging. Samples were imaged on a Zeiss
167 AxioImager.M2 with ApoTome. The TUNEL assay was performed with the ApopTag Red
168 *In Situ* Apoptosis Detection Kit (Millipore, S7165). Dissected larvae were fixed in 4%
169 paraformaldehyde, followed by a 10-minute wash in 75μL equilibration buffer. Discs were
170 then submerged in 55μL working strength TdT enzyme for 3 hours at 37°C. The reaction
171 was stopped by adding 1mL stop/wash buffer and incubating for 10 minutes at room
172 temperature, followed by 3 washes in PBS. Primary staining was done by incubating 65μL
173 of the anti-digoxygenin rhodamine overnight at room temperature.

174

175 **Quantification and Statistical Analysis**

176 Adult wing measurements were gathered using the ImageJ software. GraphPad Prism
177 9.0 was used for statistical analysis and graphical representation. Graphs depict the mean
178 of each treatment, while error bars indicate the 95% confidence interval. All experiments
179 were repeated twice. The n for each experiment is indicated in the figure legends and
180 Method Details. A One-Factor ANOVA was used to determine statistical significance,
181 while a Tukey's multiple comparisons test was chosen for post-hoc testing.

182

183 **Data and Reagent Availability**

184 Strains and plasmids are available upon request, and details of stocks and reagents
185 used in this study are available in the Reagent Table. The authors affirm that all data

186 necessary for confirming the conclusions of the article are present within the article,

187 figures, and tables.

188 **Results**

189 **A genetic method to induce necrotic injury in the wing imaginal disc**

190 To study the response to necrosis we developed a method to induce damage in the larval
191 wing disc by adapting a system we previously established to study regeneration called
192 DUAL Control (Harris et al. 2020). This system utilizes a split version of the bacterial
193 *LexA*/*lexAOp* transcriptional regulator to transiently express a pro-apoptotic gene in the
194 distal wing tissue under the control of the *spalt* (*salm*) enhancer following a short heat
195 shock (Figure 1A). This apoptosis stimulates regeneration over the subsequent ~24 to 48
196 hr, which can be quantitatively assessed by examining the degree to which the distal tip
197 of the wing is present in the adult fly (Harris et al. 2020). We previously used *lexAOp*-
198 driven *reaper* (*rpr*) to induce cell death (Harris et al. 2020), and have since established
199 another apoptosis-promoting transgene, *lexAOp-hep*^{CA}, a constitutive form of the JNK
200 kinase *hemipterous* (Adachi-Yamada et al. 1999). To study necrosis, we used the GluR1
201 protein, a murine glutamate receptor that regulates Ca^{2+} ion entry into a cell (Kohda et al.
202 2000). A characterized allele of this ion channel (*GluR1*^{LC}) confers constitutive activity,
203 leading to Ca^{2+} influx, osmotic swelling and catastrophic death of the cell (Kohda et al.
204 2000; Yang et al. 2013). We generated *lexAOp-GluR1*^{LC} and used it to build a version of
205 DUAL Control that expresses *GluR1*^{LC} in the developing wing disc (Figure 1A).

206

207 To test our ability to induce damage using this system, we heat shocked larvae bearing
208 DUAL Control expressing *GluRI*^{LC} alongside discs ablated by *rpr* or *hep*^{CA} (hereafter
209 *DC*^{GluRI}, *DC*^{rpr} and *DC*^{hepCA}), using the pouch marker *nubbin* (*nub*) and the cell adhesion
210 marker *DE-cadherin* (*DE-cad*) to evaluate disc integrity (Figure 1B). Ablation with *DC*^{GluRI}

211 leads to a loss of tissue in the *salm* domain, shown by an absence of both markers (Figure
212 1C), which is comparable to the loss of tissue resulting from ablation by DC^{rpr} (Figure 1D)
213 and DC^{hepCA} (Figure 1E). We next examined the degree to which wing discs can
214 regenerate following DC^{GluR1} ablation compared to DC^{rpr} and DC^{hepCA}. Regeneration was
215 assayed by appearance of the adult wing, scored for the presence of the distal wing tip
216 (Figure 1F and 1G) and measurement of the total wing area (Figure 1H). Ablation by DC^{rpr}
217 and DC^{hepCA} in early L3 (84 hr after egg deposition, AED) leads to significant regeneration,
218 illustrated by both wing scoring and area (Figure 1G and 1H). Ablation by DC^{GluRI} results
219 in comparable levels of ablation and regeneration (Figure 1G and 1H). The ability of discs
220 to regenerate is known to decline with developmental maturity from early to late L3 (Harris
221 et al. 2016; Harris et al. 2020). Ablation by each method in late L3 (108 hr AED) results
222 in a similar loss of distal wing tissue (Figure 1G and H). Together, these data show that
223 DC^{GluRI} can ablate the wing disc and induce regeneration comparable to apoptosis-based
224 methods.
225
226 To characterize how DC^{GluRI} induces damage we examined ablated discs for different cell
227 death markers. The loss of tissue in DC^{GluRI} coincides with strong propidium iodide (PI)
228 staining (Figure 2A, arrowhead), which labels cells with compromised membranes such
229 as those undergoing necrosis (Wlodkowic et al. 2011). Conversely, PI staining of DC^{hepCA}
230 ablated discs shows only weak and sporadic PI (Figure 2B). As activated caspases are a
231 hallmark of apoptosis rather than necrosis, we also stained ablated discs for the cleaved
232 caspase DCP1. As expected, ablation with DC^{rpr} or DC^{hepCA} yields a strong DCP1 signal
233 concentrated within the *salm* domain (Figures 2E and 2F). Sporadic caspase-positive

234 cells are seen outside of the ablation domain in all discs, likely as a result of the stress of
235 heat shock used to activate ablation (Figure 2C). Surprisingly, discs ablated with *DC*^{GluRI}
236 also have significant levels of DCP1 (Figure 2D). However, most of this staining is
237 observed in the lateral wing pouch at a distance from the ablated tissue (Figure 2D,
238 arrowheads). These DCP1 positive cells are clearly separable from the dying cells in the
239 *salm* domain. They are also not a result of dying cells moving away from the site of injury,
240 as a *lexAop-GFP* transgene that labels ablated cells fails to mark the caspase positive
241 cells outside of the *salm* domain (Figures 2G and 2H, arrowheads). This is in contrast to
242 *DC*^{hepCA} discs in which GFP and DCP1 almost entirely overlap (Figure 2I and 2J). Thus,
243 the observed apoptosis does not occur in cells killed by *GluRI* but is instead induced in
244 neighboring cells.
245
246 In addition to promoting apoptosis, caspases can perform other cellular functions in
247 imaginal discs unrelated to cell death (Su 2020). To examine whether the detected
248 caspase activity is related to cell death we also performed a TUNEL assay, which reveals
249 strong staining in the caspase positive cells found outside of the *salm* domain in *DC*^{GluRI}
250 discs (Figure 2K, arrowheads). This is consistent with *GluRI*-induced caspase activity
251 leading to cell death, as in *DC*^{rpr} and *DC*^{hepCA} ablated discs (Figure 2L and data not
252 shown). We also observed a separate weaker TUNEL signal in *GluRI* expressing cells
253 within the *salm* domain indicative of DNA fragmentation (Figure 2K, open arrowhead),
254 which has previously been described in necrotic cells (Grasl-Kraupp et al. 1995).
255 Together, these results demonstrate that ablation with *DC*^{GluR1} leads to tissue loss and

256 stimulates regeneration, but also unexpectedly activates widespread apoptosis in the
257 surrounding cells at a distance from the injury.
258
259 **Tissue loss via *DC^{GluRI}* ablation occurs independent of caspase activity**
260 To understand if the non-autonomous apoptosis observed in *DC^{GluRI}* discs contributes to
261 tissue loss, or alternatively is a consequence of it, we used the baculoviral caspase
262 inhibitor P35 to block apoptosis in the entire pouch (Hay et al. 1994). DUAL Control
263 permits the expression of UAS-driven transgenes in the wing pouch independent of
264 ablation under the control of a flip-out GAL4 (*DVE>>GAL4*), which is initiated by the same
265 heat shock that triggers ablation and persists throughout the subsequent regeneration
266 period (Figure 1A', (Harris et al. 2020). To test P35 in the DUAL Control system, we first
267 blocked apoptosis in *rpr* ablated discs using *UAS-p35* (*DC^{rpr}>>p35*). These discs have an
268 intact pouch epithelium, shown by *nub* and *DE-cad* staining (Figure 3A), and lack TUNEL
269 staining (Figure S1A). DCP1 is still detected in *DC^{rpr}>>p35* discs although the intense
270 punctate staining is replaced by a diffuse cytoplasmic signal (Figures 3C and 3D), which
271 has been reported previously when caspase activity is inhibited by P35 (Perez-Garijo et
272 al. 2013). Conversely, P35 is unable to prevent tissue loss resulting from *GluRI*
273 expression, indicated by the absence of *nub* and *DE-cadherin* in the pouch (Figure 3B)
274 and presence PI staining in the *salm* domain (Figure 3G). The appearance of the DCP1
275 staining in *DC^{GluRI}>>p35* discs is also diffuse (Figures 3E and 3F) similar to that of
276 *DC^{rpr}>>p35*, while TUNEL staining in the lateral pouch is now absent (Figure 3H),
277 indicating that the apoptosis in these regions is being blocked. However, the weak TUNEL
278 signal within the cells of the *salm* domain is still observed (Figure 3H, open arrowhead).

279 These data suggest that inhibition of caspase activity cannot block cell death or tissue
280 loss caused by GluRI within the *salm* domain.
281
282 In agreement with the observed disc phenotypes, blocking apoptosis with P35 in *rpr*
283 ablated discs results in full sized adult wings, shown by scoring and wing area
284 measurements of both early and late L3 ablated organisms (Figures 3I, 3K, 3K' and 3M).
285 By contrast, blocking apoptosis in *GluRI* ablated discs does not prevent tissue loss, as
286 adult wings that develop from DC^{GluRI}>>*p35* discs have comparable phenotypes to discs
287 ablated in the absence of P35 (Figures 3J, 3L, 3L' and 3M). Together these observations
288 suggest that GluRI can kill cells independent of caspase activity, and that the apoptotic
289 cells seen at a distance from the wound are a consequence of this tissue loss rather than
290 being required for it. Thus, we refer to DC^{GluRI}-induced tissue loss as necrotic ablation,
291 and the non-autonomous caspase-positive cell death in the surrounding tissue as
292 necrosis-induced apoptosis (NiA).
293
294 In our adult wing assays we noted a distinct category of wings from DC^{GluRI}>>*p35* animals
295 that are poorly patterned and have increased blistering and folding (Figure S1B and S1C).
296 This phenotype also occurs in DC^{hepCA}>>*p35* discs (Figure S1C). Blocking caspase
297 activity with P35 in cells undergoing apoptosis can produce undead cells that continue to
298 express mitogenic genes like *wg* and *dpp* downstream of JNK signaling, leading to
299 tumorous overgrowth of the surrounding tissue (Martin et al. 2009; Perez-Garijo et al.
300 2004; Ryoo et al. 2004). Indeed, DC^{hepCA}>>*p35* have significant ectopic *wg* expression in
301 the ablation domain overlapping the diffuse DCP1 compared to ablation in the absence

302 of P35 (Figure S1D and S1E). We hypothesized that blocking apoptosis in *DC^{GluRI}>>p35*
303 ablated discs might result in undead cells, which is responsible for the overgrown and
304 poorly patterned adult wing phenotype. However, *wg* expression appears mostly
305 unchanged in the pouch cells surrounding the wound in *DC^{GluRI}>>p35* discs (Figure S1F),
306 as does *Dpp* shown by a *Dpp-lacZ* reporter (data not shown). These data suggest that
307 undead NiA cells do not activate the same genetic pathways as undead cells generated
308 by directly activating apoptosis in the presence of P35. However, our experiments do not
309 rule out other mitogens being produced that might lead to the observed overgrowth
310 phenotype of *DC^{GluRI}>>p35* wings.
311

312 **NiA and wound edge apoptosis originate separately**

313 To investigate the origin and timing of the NiA seen in *DC^{GluRI}* discs we performed a time
314 course of ablation and regeneration (Figure 4). In order to observe the formation of the
315 wound we took advantage of the *DR^{WNT}* transgene, a damage-specific fluorescent
316 reporter of WNT expression, which is activated upon ablation and represents one of the
317 earliest signaling events in disc regeneration (Figure 4A-4F)(Harris et al. 2016). *DR^{WNT}*
318 expression starts to become apparent at the wound edge 6 hr post-ablation with GluRI
319 (Figure 4B), while most apoptotic cells in this region become obvious at around 12 hr
320 (Figure 4C, arrowhead). NiA populations are still not observed at this timepoint, but only
321 occur at 18 hr post ablation subsequent to the appearance of wound edge apoptosis and
322 *DR^{WNT}* activity (Figure 4D, arrowheads). The NiA persists as regeneration proceeds
323 (Figure 4E), and by 48 hr, when *DR^{WNT}* expression is diminished, the DCP1-positive
324 cellular debris appears to be pushed dorsally and ventrally as a result of pouch growth

325 (Figure 4F). At this time point the pouch is fully restored, indicated by *nub* expression
326 (Figure 4G). Interestingly, DR^{WNT} activity is never observed beyond the wound edge, and
327 does not occur in NiA cells. Thus, the time course shows that formation of NiA is not only
328 spatially distinct from the wound edge apoptosis and damage associated signaling shown
329 by DR^{WNT}, but is also temporally separated from it. These observations suggest that these
330 two populations might arise from different mechanisms.
331
332 **NiA is independent of JNK signaling**
333 The DR^{WNT} reporter used in the time course is directly activated by JNK signaling (Harris
334 et al. 2016). Since DR^{WNT} expression is restricted to the wound edge, and JNK signaling
335 is a key pathway that regulates both apoptosis and proliferation in response to damage
336 (Pinal et al. 2019), we next evaluated JNK signaling in DC^{GluRI} ablated discs. Using a
337 reporter for AP-1 activity (*AP-1-GFP* (Chatterjee and Bohmann 2012) we found that JNK
338 signaling is present only in wound edge cells and not in cells undergoing NiA (Figure 5A),
339 consistent with the DR^{WNT} reporter expression. Examination of the JNK target genes *puc,*
340 *wg* and *Mmp1* supports these results (Figures 5B, 5C and 5D), suggesting that necrotic
341 ablation leads to JNK upregulation and low levels of apoptosis at the wound edge, but
342 induces NiA at a distance without activating JNK.
343
344 To test whether NiA does indeed occur independent of JNK, we investigated how altering
345 different elements of the JNK pathway might influence either the wound edge or NiA
346 populations in DC^{GluRI} ablated discs. Knockdown of the JNK kinase *hep* using RNAi
347 reduces the expression of the JNK target *Mmp1* but does not strongly alter apoptosis at

348 the wound edge (Figure 5E). Importantly, NiA cells are still observed in the absence of
349 *hep* (Figure 5E). This result is confirmed using a *hep* hemizygous mutant (*hep*^{r75}/*Y*),
350 although the level of apoptosis across the whole disc is somewhat reduced when using
351 this allele (Figure S2A). The expression of a dominant negative form of the JNK *basket*
352 (*UAS-bsk*^{DN}) strongly suppresses *Mmp1* expression (Figure 5F), and unlike the loss of
353 *hep*, *bsk*^{DN} also reduces apoptosis at the wound edge (Figure 5F), suggesting that this
354 cell death is dependent on *bsk*. The population of NiA cells is also unaffected in this
355 background (Figure 5F), supporting the idea that NiA formation does not depend on JNK
356 signaling. RNAi knockdown of *bsk* also confirms these results (Figure S2B). Since the
357 loss of *bsk*, but not *hep*, seems to influence wound edge apoptosis, we also targeted an
358 alternative JNK kinase, *Mkk4*, for knockdown in *DC*^{GluRI} ablated discs. Unlike *hep*,
359 reduction of *Mkk4* levels reduces both the apoptosis and *Mmp1* expression at the wound
360 edge, but again has no influence on the appearance of NiA (Figure 5G). We also reduced
361 expression of the TNF receptor *grindlewald* (*grnd*) and TNF ligand *egr* using RNAi.
362 Neither manipulation affected the apoptosis or JNK activity at the wound edge or the
363 appearance of the cells undergoing NiA outside the ablated domain (Figure S2C and
364 S2D). Moreover, a reporter for *egr* expression (*egr-GAL4, UAS-GFP*) shows no
365 upregulation of *egr* at the wound edge or in cells undergoing NiA (Figure S2E and S2F).
366 Overall, these data suggest that necrotic ablation induces low levels of apoptosis and
367 JNK signaling at the wound edge, which occurs downstream of the JNK receptor and is
368 dependent on both *Mkk4* and *bsk*, while also generating NiA at a distance via a JNK-
369 independent signal.
370

371 As NiA does not appear to require JNK, we sought to investigate factors upstream of the
372 observed activated caspase DCP1 that might be required for the production of NiA
373 following necrotic ablation. We used an RNAi targeting the dIAP1 inhibitor *rpr*, which
374 activates cell death immediately upstream of initiator caspases. Knockdown of *rpr* leads
375 to a moderate reduction in apoptosis at the wound edge, but importantly also reduces NiA
376 formation (Figure S2G). When a miRNA targeting *rpr* and the two additional dIAP1
377 inhibitors *hid* and *grim* was used (*UAS-miRHG*), NiA formation was eliminated (Figure
378 5H), as was the cell death normally observed at the wound edge, indicating that more
379 than one of these genes are required for both wound edge apoptosis and NiA. Importantly,
380 DC^{GluRI}-induced tissue loss still clearly occurs even in the absence of NiA (Figure S2H),
381 while JNK signaling shown by *Mmp1* expression is still observed (Figure 5H). Thus,
382 necrotic ablation leads to apoptosis at the wound edge and NiA in the surrounding pouch,
383 and although they both rely on the same downstream factors to ultimately cause cell
384 death, each appears to be induced by a different activating signal.
385

386 **NiA is required for blastema formation and promotes regeneration**

387 To understand the potential contribution of NiA to regeneration we examined how the
388 appearance of NiA coincides with blastema formation following necrotic ablation. We
389 used a reporter for *E2F* (*PCNA-GFP*) and *Cyclin E* (*cycE-GFP*) to examine changes in
390 proliferation that occur following ablation and during regeneration (Smith-Bolton et al.
391 2009). These markers show that proliferation induced by necrotic ablation does not
392 significantly increase in the wing pouch until around 24 hr, after the formation of NiA at
393 18 hr (Figure 6A, 6B, S3A, and S3B). To test whether NiA has a role in blastema formation

394 we sought to eliminate this apoptosis following *DC*^{GluRI} ablation. As NiA is unaffected by
395 blocking JNK signaling, and P35 allows dying cells to persist in the disc which could
396 complicate our analysis, we used *UAS-miRHG* to prevent the formation of NiA. The lack
397 of NiA in the pouch following necrotic ablation results in a loss of *PCNA-GFP* upregulation
398 that is normally seen at 24 hr (Figure 6C), suggesting that NiA is required for blastema
399 formation. Importantly, JNK signaling at the wound edge is still observed following *miRHG*
400 expression, indicated by the presence of *Mmp1* (Figure 6C), demonstrating that blastema
401 formation following necrotic ablation is not dependent solely on JNK activity from the
402 wound, but also requires NiA.
403
404 Finally, we examined how blocking NiA might influence the discs capacity to regenerate.
405 Evaluating adult wings that develop from *DC*^{GluRI}*>>miRHG* discs shows they have a
406 reduced ability to regenerate compared to control discs (Figure 6E and 6F). This result is
407 significant, as blocking apoptosis with *miRHG* would normally be expected to improve
408 regeneration, as it does in *DC*^{rpr} ablated discs (Figure 6D and 6F). Together, these results
409 show that NiA is required for the formation of a blastema to promote regeneration in
410 response to necrosis.
411
412 **Discussion**
413 **Necrosis induces apoptosis at a distance in the wing imaginal disc**
414 Necrotic ablation induces apoptosis in cells in two regions of the injured disc: at the wound
415 edge and more extensively in the surrounding pouch. These two populations of dying
416 cells are likely induced by separate mechanisms and contribute differently to regeneration

417 (Figure 7). The wound edge apoptosis coincides with JNK activity and is likely dependent
418 on it, as interference with *bsk* strongly limits the caspase observed at the wound. The
419 factors that can activate JNK signaling, and those downstream that regulate whether cells
420 subsequently proliferate or undergo apoptosis, are complex and context dependent (La
421 Marca and Richardson 2020; Pinal et al. 2019). However, our experiments show that
422 pathway activation following necrotic ablation occurs downstream of the receptor *grnd*
423 and relies on the JNK kinase *Mkk4* more than *hep*. There are a number of signals that
424 can induce JNK activity in this way, including loss of polarity, mechanical inputs and the
425 release of immediate stress signals such as reactive oxygen species (ROS)(La Marca
426 and Richardson 2020). ROS has been shown to upregulate both JNK and P38, another
427 factor that regulates proliferation and apoptosis, via Ask1/AKT (Santabarbara-Ruiz et al.
428 2019; Santabarbara-Ruiz et al. 2015), while ROS is known to be an important regulator
429 of regeneration in the wing disc (Brock et al. 2017; Khan et al. 2017; Santabarbara-Ruiz
430 et al. 2019; Santabarbara-Ruiz et al. 2015). Thus, it is possible that the JNK signaling and
431 associated apoptosis at the wound edge induced by necrotic ablation is mediated via this
432 pathway. It is likely that this JNK activity contributes to recovery following necrosis, as it
433 does in apoptosis-induced regeneration. However, our observation that blocking NiA
434 limits regeneration, despite wound edge JNK being unaffected, suggests that
435 regeneration does not solely depend on it.
436
437 The signals that lead to the NiA at a distance from the necrotic injury are less clear,
438 however. A related phenomenon to the one we have observed, in which cells undergoing
439 programmed cell death induce additional non-autonomous apoptosis, has been

440 described in the wing imaginal disc and the mouse hair follicle (Perez-Garijo et al. 2013).
441 However, in both contexts these events are induced by apoptotic cell death rather than
442 necrosis, and are mediated by JNK signaling, unlike the formation of NiA. In a parallel
443 observation to that of apoptotic cells communicating with surrounding tissues, studies
444 have shown that cells undergoing necrosis might also release factors that regulate the
445 behavior of neighboring cells. These factors are collectively known as damage associated
446 molecular patterns or DAMPs (Gong et al. 2020; Roh and Sohn 2018). Such signals often
447 consist of endogenous intracellular molecules like cytoskeletal components, DNA, RNA,
448 histones and metabolites, which are passively released and inappropriately exposed to
449 the extracellular environment. DAMPs are detected by immune cells that in turn activate
450 immune pathways to mount a stress response, known as sterile inflammation (Gong et
451 al. 2020). Beyond these initial inflammatory responses, DAMPs are also important for
452 orchestrating the subsequent steps in tissue repair and regeneration (Venereau et al.
453 2015). In *Drosophila*, the actin-binding protein α-actinin has been shown to act as a
454 DAMP when purified and injected into adult flies, inducing a humoral immune response
455 in the form of cytokine signal activation specifically in the fat body (Gordon et al. 2018;
456 Srinivasan et al. 2016). Similarly, apoptotic-deficient *Drosophila* constitutively activate
457 immune signaling in the larval fat body due to the presence of circulating DAMPs in the
458 hemolymph (Ming et al. 2014). Recently it was shown that imaginal disc damage leads to
459 the upregulation of circulating metabolites produced by the fat body, which are necessary
460 for proper disc repair (Kashio and Miura 2020), highlighting the importance of this
461 interorgan communication in the context of regeneration. Thus, one possibility is that
462 necrotic cells release DAMP signals to induce pro-regenerative NiA in the disc via an

463 immune response involving the fat body. The role of hemocytes, an essential population
464 of immune cells, in the regeneration of damaged imaginal discs has also been explored
465 following physical and apoptotic damage (Fogarty et al. 2016; Katsuyama and Paro 2013;
466 Pastor-Pareja et al. 2008), and in the context of sterile inflammation that occurs following
467 necrosis (Shaukat et al. 2015). Considering the vital roles hemocytes play in these
468 processes it is possible they also mediate immune or other signals to induce NiA
469 formation. Alternatively, DAMPs are also known to have stimulatory effects on non-
470 immune cells (Chen and Nunez 2010; Gong et al. 2020), and thus could be sensed
471 directly by the immediately surrounding pouch tissues to induce NiA. Going forward it will
472 be important to identify the both the identity of the signal and the physiological mechanism
473 by which necrosis leads to non-autonomous cell death in the wing disc.
474

475 **NiA is necessary for blastema formation and subsequent regeneration**

476 Our data show that blocking apoptosis following necrosis restricts blastema formation and
477 limits regeneration, strongly suggesting that NiA is a vital part of the recovery process.
478 How this type of cell death might promote proliferation is still unclear, however. Apoptosis-
479 induced proliferation (AiP) is a well-established phenomenon, in which dying cells release
480 mitogens, such as *wg* and *dpp*, downstream of JNK signaling to stimulate localized
481 proliferation (Fogarty and Bergmann 2017; Perez-Garijo and Steller 2015). These
482 mitogens act via a feed forward mechanism that involves the release of ROS, recruitment
483 of hemocytes and induction of further JNK signaling to promote repair (Fogarty and
484 Bergmann 2017; Fogarty et al. 2016). By contrast, we have shown that cells undergoing
485 NiA do not detectably express *wg* or *dpp*, even in an undead state, and do not activate

486 JNK signaling. Although we have not ruled out other characterized mitogens being
487 involved, these findings suggest that NiA may not promote proliferation via the
488 established AiP mechanism. An important consideration is whether cells undergoing NiA
489 release specific signals to direct tissue regrowth, as seen with AiP, or if the tissue loss
490 resulting from necrosis and NiA is instead sensed more generally at the level of the whole
491 disc, stimulating coordinated regrowth in addition to localized proliferation (Hariharan
492 2015). The identification of signals produced by NiA cells and a better understanding of
493 proliferation rates across a recovering disc will help to reveal the contribution of these
494 different mechanisms to necrosis-induced regeneration.
495
496 Tissue necrosis is associated with many types of traumatic injury and diseases in
497 humans, including ischemic injuries, infections and cancer. Using model systems, like the
498 one we have developed here, to understand how necrotic cells impact neighboring
499 healthy tissues, and how these tissues enact mechanisms to effectively recover, may help
500 to identify therapeutic interventions that promote healing in tissues which otherwise
501 struggle to recover from necrosis, such as those of humans.

502 **References**

503 Adachi-Yamada T, Fujimura-Kamada K, Nishida Y, Matsumoto K. 1999. Distortion of
504 proximodistal information causes jnk-dependent apoptosis in drosophila wing.
505 Nature. 400(6740):166-169.
506 Beira JV, Paro R. 2016. The legacy of drosophila imaginal discs. Chromosoma.
507 125(4):573-592.
508 Bergmann A, Steller H. 2010. Apoptosis, stem cells, and tissue regeneration. Sci Signal.
509 3(145):re8.
510 Bilak A, Uyetake L, Su TT. 2014. Dying cells protect survivors from radiation-induced cell
511 death in drosophila. PLoS Genet. 10(3):e1004220.
512 Bonne SL, Kadri SS. 2017. Evaluation and management of necrotizing soft tissue
513 infections. Infect Dis Clin North Am. 31(3):497-511.
514 Brock AR, Seto M, Smith-Bolton RK. 2017. Cap-n-collar promotes tissue regeneration by
515 regulating ros and jnk signaling in the drosophila melanogaster wing imaginal disc.
516 Genetics. 206(3):1505-1520.
517 Chatterjee N, Bohmann D. 2012. A versatile phic31 based reporter system for measuring
518 ap-1 and nrf2 signaling in drosophila and in tissue culture. PLoS One. 7(4):e34063.
519 Chen GY, Nunez G. 2010. Sterile inflammation: Sensing and reacting to damage. Nat
520 Rev Immunol. 10(12):826-837.
521 Chera S, Ghila L, Dobretz K, Wenger Y, Bauer C, Buzgariu W, Martinou JC, Galliot B.
522 2009. Apoptotic cells provide an unexpected source of wnt3 signaling to drive
523 hydra head regeneration. Developmental cell. 17(2):279-289.
524 Fogarty CE, Bergmann A. 2015. The sound of silence: Signaling by apoptotic cells. Curr
525 Top Dev Biol. 114:241-265.
526 Fogarty CE, Bergmann A. 2017. Killers creating new life: Caspases drive apoptosis-
527 induced proliferation in tissue repair and disease. Cell Death Differ. 24(8):1390-
528 1400.
529 Fogarty CE, Diwanji N, Lindblad JL, Tare M, Amcheslavsky A, Makhijani K, Bruckner K,
530 Fan Y, Bergmann A. 2016. Extracellular reactive oxygen species drive apoptosis-
531 induced proliferation via drosophila macrophages. Curr Biol. 26(5):575-584.

532 Fox DT, Cohen E, Smith-Bolton R. 2020. Model systems for regeneration: Drosophila.
533 Development. 147(7).
534 Fuchs Y, Steller H. 2011. Programmed cell death in animal development and disease.
535 Cell. 147(4):742-758.
536 Fuchs Y, Steller H. 2015. Live to die another way: Modes of programmed cell death and
537 the signals emanating from dying cells. Nat Rev Mol Cell Biol. 16(6):329-344.
538 Gong T, Liu L, Jiang W, Zhou R. 2020. Damp-sensing receptors in sterile inflammation
539 and inflammatory diseases. Nat Rev Immunol. 20(2):95-112.
540 Gordon O, Henry CM, Srinivasan N, Ahrens S, Franz A, Deddouche S, Chakravarty P,
541 Phillips D, George R, Kjaer S et al. 2018. Alpha-actinin accounts for the bioactivity
542 of actin preparations in inducing stat target genes in drosophila melanogaster.
543 Elife. 7.
544 Grasl-Kraupp B, Ruttkay-Nedecky B, Koudelka H, Bukowska K, Bursch W, Schulte-
545 Hermann R. 1995. In situ detection of fragmented DNA (tunel assay) fails to
546 discriminate among apoptosis, necrosis, and autolytic cell death: A cautionary
547 note. Hepatology. 21(5):1465-1468.
548 Hacker G. 2018. Apoptosis in infection. Microbes Infect. 20(9-10):552-559.
549 Hakkarainen TW, Kopari NM, Pham TN, Evans HL. 2014. Necrotizing soft tissue
550 infections: Review and current concepts in treatment, systems of care, and
551 outcomes. Curr Probl Surg. 51(8):344-362.
552 Hariharan IK. 2015. Organ size control: Lessons from drosophila. Developmental cell.
553 34(3):255-265.
554 Hariharan IK, Serras F. 2017. Imaginal disc regeneration takes flight. Curr Opin Cell Biol.
555 48:10-16.
556 Harris RE, Setiawan L, Saul J, Hariharan IK. 2016. Localized epigenetic silencing of a
557 damage-activated wnt enhancer limits regeneration in mature drosophila imaginal
558 discs. Elife. 5.
559 Harris RE, Stinchfield MJ, Nystrom SL, McKay DJ, Hariharan IK. 2020. Damage-
560 responsive, maturity-silenced enhancers regulate multiple genes that direct
561 regeneration in drosophila. Elife. 9.

562 Hay BA, Wolff T, Rubin GM. 1994. Expression of baculovirus p35 prevents cell death in
563 drosophila. Development. 120(8):2121-2129.
564 Huh JR, Guo M, Hay BA. 2004. Compensatory proliferation induced by cell death in the
565 drosophila wing disc requires activity of the apical cell death caspase dronc in a
566 nonapoptotic role. Curr Biol. 14(14):1262-1266.
567 Kashio S, Miura M. 2020. Kynurenine metabolism in the fat body non-autonomously
568 regulates imaginal disc repair in drosophila. iScience. 23(12):101738.
569 Katsuyama T, Paro R. 2013. Innate immune cells are dispensable for regenerative growth
570 of imaginal discs. Mech Dev. 130(2-3):112-121.
571 Khan SJ, Abidi SNF, Skinner A, Tian Y, Smith-Bolton RK. 2017. The drosophila duox
572 maturation factor is a key component of a positive feedback loop that sustains
573 regeneration signaling. PLoS Genet. 13(7):e1006937.
574 Kohda K, Wang Y, Yuzaki M. 2000. Mutation of a glutamate receptor motif reveals its role
575 in gating and delta2 receptor channel properties. Nat Neurosci. 3(4):315-322.
576 Konstantinidis K, Whelan RS, Kitsis RN. 2012. Mechanisms of cell death in heart disease.
577 Arterioscler Thromb Vasc Biol. 32(7):1552-1562.
578 La Marca JE, Richardson HE. 2020. Two-faced: Roles of jnk signalling during
579 tumourigenesis in the drosophila model. Front Cell Dev Biol. 8:42.
580 Li F, Huang Q, Chen J, Peng Y, Roop DR, Bedford JS, Li CY. 2010. Apoptotic cells
581 activate the "phoenix rising" pathway to promote wound healing and tissue
582 regeneration. Sci Signal. 3(110):ra13.
583 Liu K, Ding L, Li Y, Yang H, Zhao C, Lei Y, Han S, Tao W, Miao D, Steller H et al. 2014.
584 Neuronal necrosis is regulated by a conserved chromatin-modifying cascade. Proc
585 Natl Acad Sci U S A. 111(38):13960-13965.
586 Martin FA, Perez-Garijo A, Morata G. 2009. Apoptosis in drosophila: Compensatory
587 proliferation and undead cells. Int J Dev Biol. 53(8-10):1341-1347.
588 Masi L, Falchetti A, Brandi ML. 2007. Osteonecrosis in genetic disorders. Clin Cases
589 Miner Bone Metab. 4(1):27-29.
590 Milner PF, Kraus AP, Sebes JI, Sleeper LA, Dukes KA, Embury SH, Bellevue R, Koshy
591 M, Moohr JW, Smith J. 1991. Sickle cell disease as a cause of osteonecrosis of
592 the femoral head. N Engl J Med. 325(21):1476-1481.

593 Ming M, Obata F, Kuranaga E, Miura M. 2014. Persephone/spatzle pathogen sensors
594 mediate the activation of toll receptor signaling in response to endogenous danger
595 signals in apoptosis-deficient drosophila. J Biol Chem. 289(11):7558-7568.
596 Pastor-Pareja JC, Wu M, Xu T. 2008. An innate immune response of blood cells to tumors
597 and tissue damage in drosophila. Dis Model Mech. 1(2-3):144-154; discussion
598 153.
599 Pellettieri J, Fitzgerald P, Watanabe S, Mancuso J, Green DR, Sanchez Alvarado A.
600 2010. Cell death and tissue remodeling in planarian regeneration. Dev Biol.
601 338(1):76-85.
602 Perez-Garijo A, Fuchs Y, Steller H. 2013. Apoptotic cells can induce non-autonomous
603 apoptosis through the tnf pathway. Elife. 2:e01004.
604 Perez-Garijo A, Martin FA, Morata G. 2004. Caspase inhibition during apoptosis causes
605 abnormal signalling and developmental aberrations in drosophila. Development.
606 131(22):5591-5598.
607 Perez-Garijo A, Steller H. 2015. Spreading the word: Non-autonomous effects of
608 apoptosis during development, regeneration and disease. Development.
609 142(19):3253-3262.
610 Pinal N, Calleja M, Morata G. 2019. Pro-apoptotic and pro-proliferation functions of the
611 jnk pathway of drosophila: Roles in cell competition, tumorigenesis and
612 regeneration. Open Biol. 9(3):180256.
613 Radak D, Katsiki N, Resanovic I, Jovanovic A, Sudar-Milovanovic E, Zafirovic S, Mousad
614 SA, Isenovic ER. 2017. Apoptosis and acute brain ischemia in ischemic stroke.
615 Curr Vasc Pharmacol. 15(2):115-122.
616 Roh JS, Sohn DH. 2018. Damage-associated molecular patterns in inflammatory
617 diseases. Immune Netw. 18(4):e27.
618 Ryoo HD, Gorenc T, Steller H. 2004. Apoptotic cells can induce compensatory cell
619 proliferation through the jnk and the wingless signaling pathways. Developmental
620 cell. 7(4):491-501.
621 Santabarbara-Ruiz P, Esteban-Collado J, Perez L, Viola G, Abril JF, Milan M, Corominas
622 M, Serras F. 2019. Ask1 and akt act synergistically to promote ros-dependent
623 regeneration in drosophila. PLoS Genet. 15(1):e1007926.

624 Santabarbara-Ruiz P, Lopez-Santillan M, Martinez-Rodriguez I, Binagui-Casas A, Perez
625 L, Milan M, Corominas M, Serras F. 2015. Ros-induced jnk and p38 signaling is
626 required for unpaired cytokine activation during drosophila regeneration. PLoS
627 Genet. 11(10):e1005595.
628 Shaukat Z, Liu D, Gregory S. 2015. Sterile inflammation in drosophila. Mediators Inflamm.
629 2015:369286.
630 Smith-Bolton RK, Worley MI, Kanda H, Hariharan IK. 2009. Regenerative growth in
631 drosophila imaginal discs is regulated by wingless and myc. Developmental cell.
632 16(6):797-809.
633 Srinivasan N, Gordon O, Ahrens S, Franz A, Deddouche S, Chakravarty P, Phillips D,
634 Yunus AA, Rosen MK, Valente RS et al. 2016. Actin is an evolutionarily-conserved
635 damage-associated molecular pattern that signals tissue injury in drosophila
636 melanogaster. Elife. 5.
637 Su TT. 2015. Non-autonomous consequences of cell death and other perks of being
638 metazoan. AIMS Genet. 2(1):54-69.
639 Su TT. 2020. Non-apoptotic roles of apoptotic proteases: New tricks for an old dog. Open
640 Biol. 10(8):200130.
641 Suzanne M, Steller H. 2013. Shaping organisms with apoptosis. Cell Death Differ.
642 20(5):669-675.
643 Tseng AS, Adams DS, Qiu D, Koustubhan P, Levin M. 2007. Apoptosis is required during
644 early stages of tail regeneration in xenopus laevis. Dev Biol. 301(1):62-69.
645 Venereau E, Ceriotti C, Bianchi ME. 2015. Damps from cell death to new life. Front
646 Immunol. 6:422.
647 Vriz S, Reiter S, Galliot B. 2014. Cell death: A program to regenerate. Curr Top Dev Biol.
648 108:121-151.
649 Wlodkowic D, Telford W, Skommer J, Darzynkiewicz Z. 2011. Apoptosis and beyond:
650 Cytometry in studies of programmed cell death. Methods Cell Biol. 103:55-98.
651 Wong RS. 2011. Apoptosis in cancer: From pathogenesis to treatment. J Exp Clin Cancer
652 Res. 30:87.
653 Worley MI, Setiawan L, Hariharan IK. 2012. Regeneration and transdetermination in
654 drosophila imaginal discs. Annu Rev Genet. 46:289-310.

655 Yang Y, Hou L, Li Y, Ni J, Liu L. 2013. Neuronal necrosis and spreading death in a
656 drosophila genetic model. Cell Death Dis. 4:e723.
657 Yuan J. 2009. Neuroprotective strategies targeting apoptotic and necrotic cell death for
658 stroke. Apoptosis. 14(4):469-477.
659

660 **Acknowledgements**

661 The authors would like to thank Dr. David Bilder and Dr. Iswar Hariharan of UC Berkeley
662 and Dr. Tian Xie of the Stowers Institute for their gift of stocks. We thank current members
663 of the Harris lab for useful feedback. We thank the Bloomington Stock Center,
664 Developmental Studies Hybridoma Bank, and BestGene for stocks, reagents, and
665 services.

666

667 **Funding Information**

668 The funders had no role in study design, data collection and interpretation, or the decision
669 to submit the work for publication. This work was supported by a grant from the NICHD 1
670 R21 HD102765-01 to Robin Harris.

671

672 **Competing interests**

673 No competing interests declared.

Figure 1

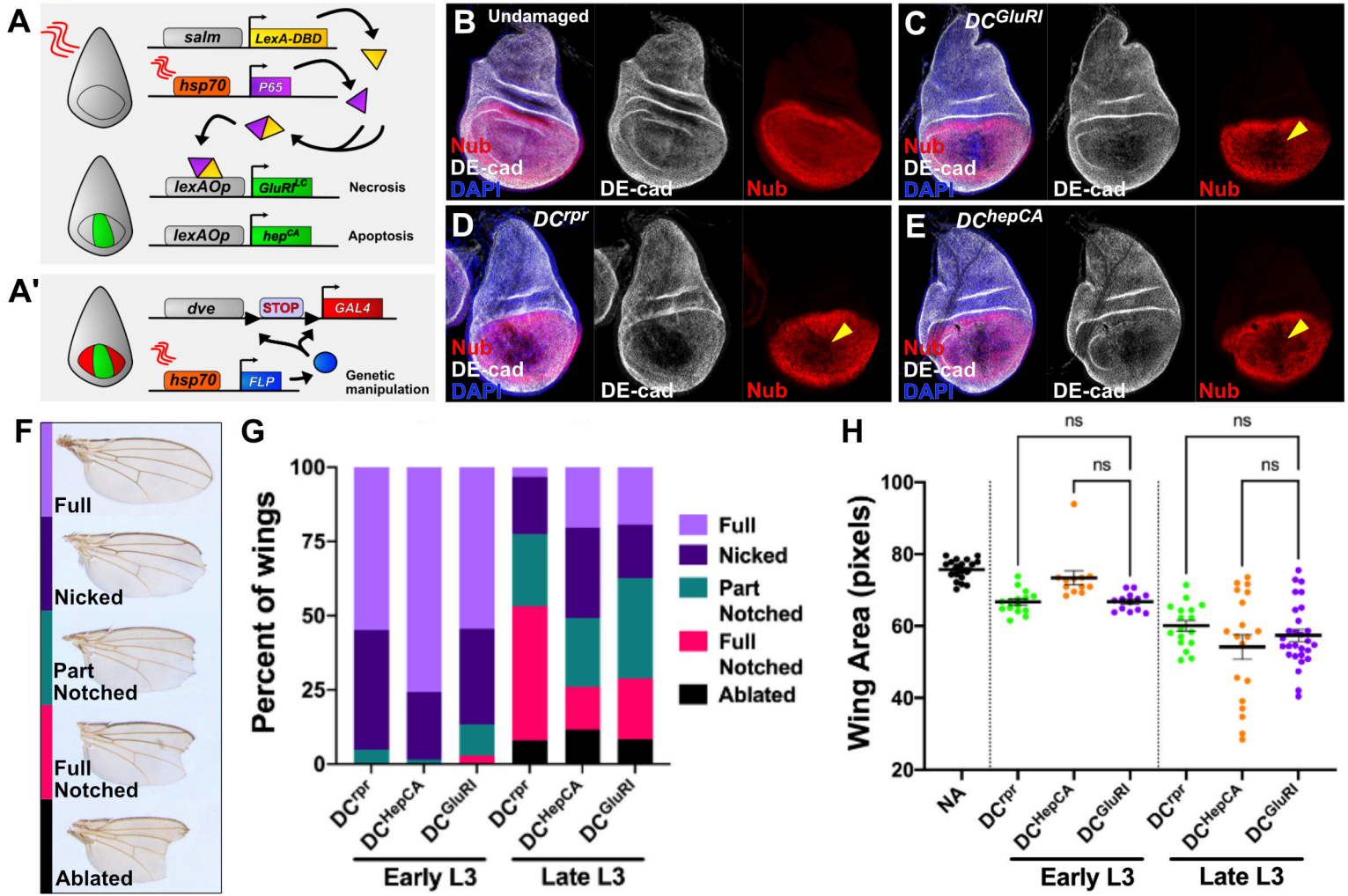
A
salm
LexA-DBD
hsp70
P65
lexAOp
GluRI^LC
Necrosis
lexAOp
hep^CA
Apoptosis
A'
dve
STOP
GAL4
hsp70
FLP
Genetic manipulation
B Undamaged
C DC^GluRI
D DC^rpr
E DC^hepCA
Nub
DE-cad
DAPI
F
Full
Nicked
Part Notched
Full Notched
Ablated
G
Percent of wings
100
75
50
25
0
Full
Nicked
Part Notched
Full Notched
Ablated
DC^rpr
DC^HepCA
DC^GluRI
Early L3
Late L3
H
Wing Area (pixels)
100
80
60
40
20
ns
NA
DC^rpr
DC^HepCA
DC^GluRI
Early L3
Late L3

674 **Figure Legends**

675 **Figure 1. *Drosophila* wing imaginal discs regenerate comparably following**

676 **ablation with DC^{rpr}, DC^{hepCA} and DC^{GluR1}.**

677 (**A-A'**) A schematic of the DUAL Control genetic ablation system, based on a split LexA

678 transcriptional activator which can form a complete transcriptional activator

679 (yellow/purple protein) using complementary leucine zipper domains following a heat

680 shock, inducing *lexAOp*-driven ablation in the *salm* domain (green area of disc) (**A**), with

681 the *DVE>>Gal4* driver used to drive *UAS*-based transgenes in the wing pouch

682 independent of ablation (red area of disc) (**A'**). *salm*: *spalt* enhancer, *DBD: DNA Binding*

683 *Domain*, *dve*: *defective proventriculus* enhancer.

684 (**B-E**) Wing discs stained for the Nubbin pouch marker (Nub, red) and DE-cadherin (DE-

685 cad, gray) in an unablated control (**B**) and following ablation with DC^{GluR1} (**C**), DC^{rpr} (**D**),

686 and DC^{hepCA} (**E**). DAPI, blue. Arrowheads in (**C-E**) indicate loss of Nub pouch marker.

687 (**F**) Adult wing ablation phenotypes following DUAL Control ablation (see also Harris et

688 al., 2020).

689 (**G**) Regeneration scoring of adult wings from early L3 discs ablated by DC^{rpr} (n = 62),

690 DC^{hepCA} (n = 66), and DC^{GluR1} (n = 68), and late L3 discs ablated by DC^{rpr} (n = 62),

691 DC^{hepCA} (n = 69), and DC^{GluR1} (n = 83).

692 (**H**) Mean pixel area of adult wings from early L3 ablated wings in an unablated control

693 (NA, n = 19), DC^{rpr} (n = 22), DC^{hepCA} (n = 12), and DC^{GluR1} (n = 17). ns, not significant.

694 Data analyzed using one-factor ANOVA and Tukey's multiple comparisons test.

Figure 2

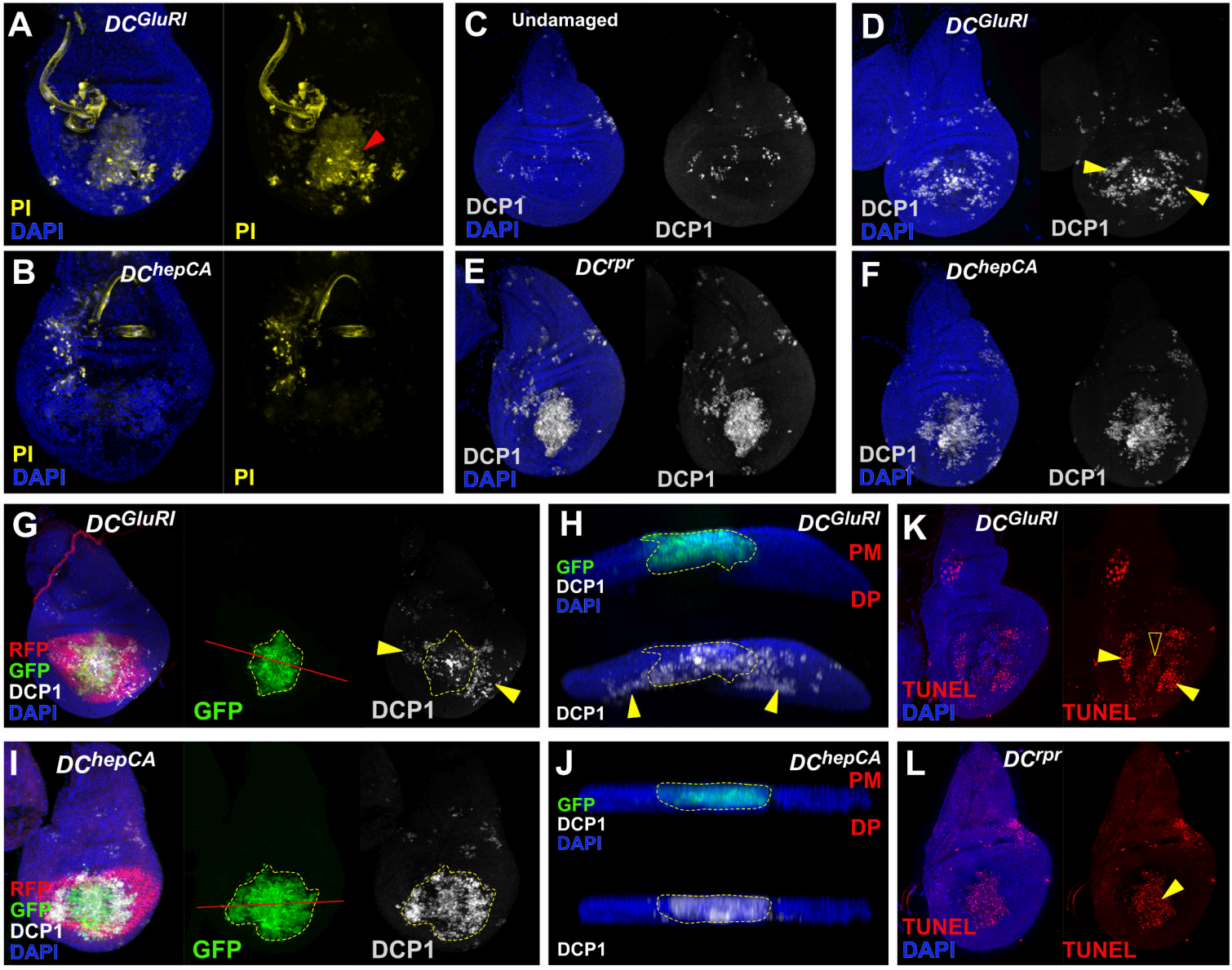
A
DCGluRI
PI
DAPI
PI
B
DChepCA
PI
DAPI
PI
C
Undamaged
DCP1
DAPI
DCP1
D
DCGluRI
DCP1
DAPI
DCP1
E
DCrpr
DCP1
DAPI
DCP1
F
DChepCA
DCP1
DAPI
DCP1
G
DCGluRI
RFP
GFP
DCP1
DAPI
GFP
DCP1
H
DCGluRI
GFP
DCP1
DAPI
PM
DP
DCP1
K
DCGluRI
TUNEL
DAPI
TUNEL
I
DChepCA
RFP
GFP
DCP1
DAPI
GFP
DCP1
J
DChepCA
GFP
DCP1
DAPI
PM
DP
DCP1
L
DCrpr
TUNEL
DAPI
TUNEL

695 **Figure 2: Ablation with *DC^{GluR1}* generates significant apoptosis at a distance.**

696 (**A-B**) Propidium iodide (PI) staining (yellow) of *DC^{GluR1}* (**A**) and *DC^{hepCA}* (**B**) ablated
697 wing discs, arrowhead in (A) indicates PI-stained dying cells in the *salm* domain of the
698 pouch. Non-specific PI staining of tracheal tubes is observed in both samples. DAPI,
699 blue.

700 (**C-F**) Caspase staining (DCP1, gray) of wing imaginal discs in a control unablated heat
701 shocked disc (**C**), and following ablation with *DC^{GluR1}* (**D**), *DC^{rpr}* (**E**), and *DC^{hepCA}* (**F**).
702 DAPI, blue. Arrowheads in (D) indicate non-autonomous caspase outside of the ablation
703 domain.

704 (**G-J**) Wing imaginal discs bearing the *lexAOp-GFP; UAS-RFP* reporter and ablated with
705 *DC^{GluR1}* (**G-H**) or *DC^{hepCA}* (**I-J**). GFP (green) labels the *salm* ablation domain, RFP (red)
706 labels the surrounding unablated pouch, and DCP1 (gray) labels apoptotic cells, DAPI,
707 blue. (**G**) Discs ablated with *DC^{GluR1}* shows DCP1-positive cells outside of the ablation
708 domain (arrowheads), red line indicates transverse section shown in (H). (**H**) A
709 transverse section through the pouch of the disc in (G) confirms that these lateral
710 DCP1-positive cells are not labeled with GFP. (**I**) Ablation by *DC^{hepCA}* shows almost
711 complete overlap between the GFP and DCP1 signals, red line indicates transverse
712 section shown in (J). (**J**) A transverse section of the disc in (I) confirming significant
713 overlap of GFP and DCP1. PM: peripodial membrane, DP: disc proper.

714 (**K-L**) TUNEL-labeling (red) of wing discs ablated with *DC^{GluR1}* (**K**) and *DC^{rpr}* (**L**). Solid
715 arrowheads indicate strong TUNEL staining in both panels, open arrowhead in (K)
716 indicates weak TUNEL staining present in the *salm* domain.

Figure 3

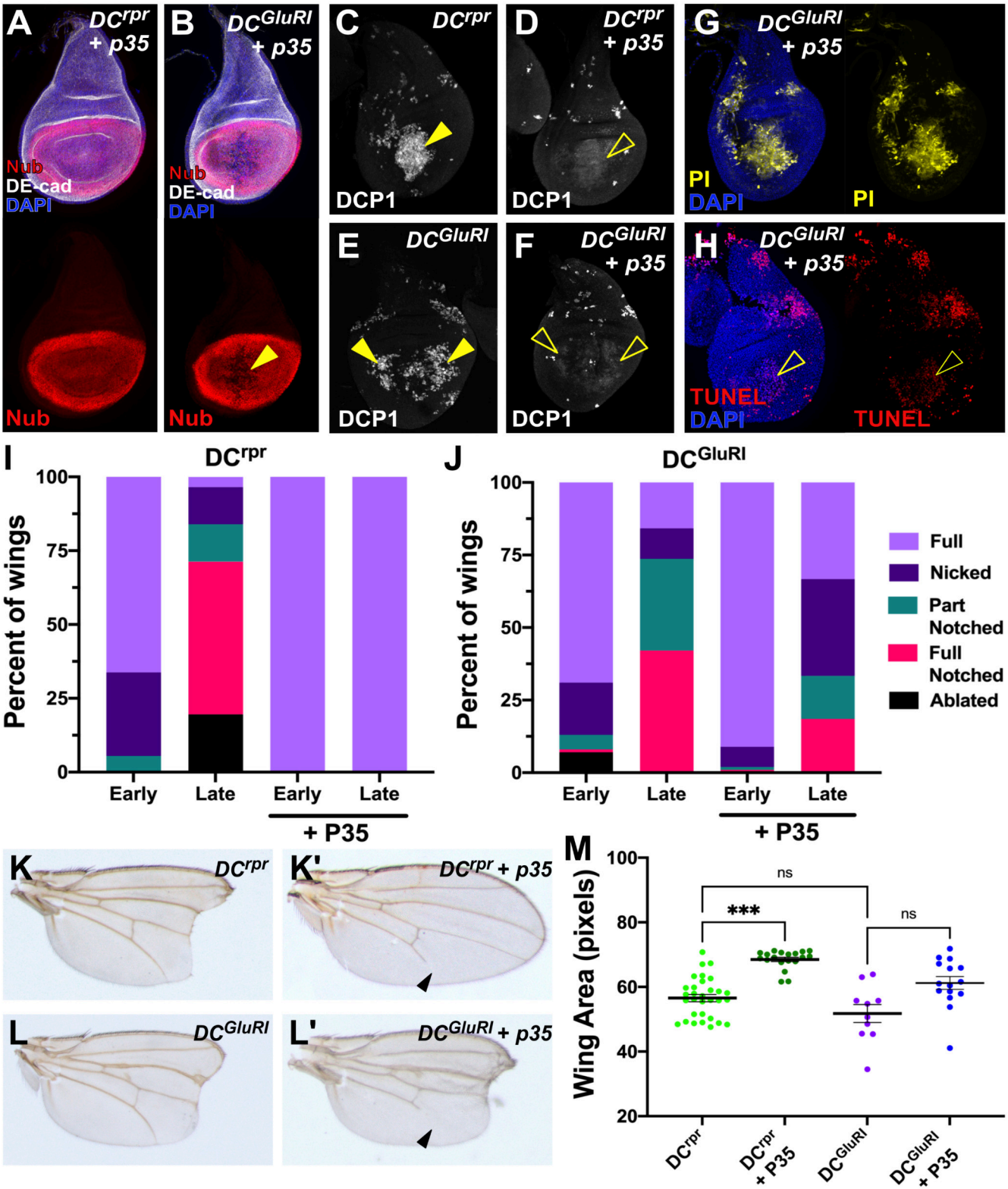
A
DCrpr + p35
Nub
DE-cad
DAPI
Nub
B
DCGluRI + p35
Nub
DE-cad
DAPI
Nub
C
DCrpr
DCP1
D
DCrpr + p35
DCP1
E
DCGluRI
DCP1
F
DCGluRI + p35
DCP1
G
DCGluRI + p35
PI
DAPI
PI
H
DCGluRI + p35
TUNEL
DAPI
TUNEL
I
DCrpr
Percent of wings
100
75
50
25
0
Early
Late
Early
Late
+ P35
J
DCGluRI
Percent of wings
100
75
50
25
0
Early
Late
Early
Late
+ P35
Full
Nicked
Part Notched
Full Notched
Ablated
K
DCrpr
K'
DCrpr + p35
L
DCGluRI
L'
DCGluRI + p35
M
Wing Area (pixels)
100
80
60
40
20
ns
***
ns
DCrpr
DCrpr + P35
DCGluRI
DCGluRI + P35

717 **Figure 3. Inhibition of caspase activity fails to prevent ablation in DC^{GluR1} discs.**

718 (**A-B**) Wing discs stained for Nub (red), DE-cad (gray), and DAPI (blue) following

719 ablation with *DC^{rpr}>>p35* (**A**) and *DC^{GluR1}>>p35* (**B**). Loss of tissue by *GluRI* ablation in

720 the presence of P35 is indicated by the arrowhead in (B).

721 (**C-F**) DCP1 staining (gray) in wing discs ablated with *DC^{rpr}* (**C**), *DC^{rpr}>>p35* (**D**), *DC^{GluR1}*

722 (**E**), *DC^{GluR1}>>p35* (**F**). The arrowheads indicate strong DCP1 staining in the ablated

723 *salm* domain in (C) and non-autonomous apoptosis in (E), while the open arrowheads in

724 (D) and (F) indicate the diffuse, cytoplasmic DCP1 staining in these populations that

725 occurs in the presence of P35.

726 (**G**) PI staining (yellow) of a *DC^{GluR1}>>p35* ablated wing disc. Non-specific PI staining of

727 the tracheal tube is observed. DAPI, blue.

728 (**H**) TUNEL-labelling (red) of a *DC^{GluR1}>>p35* ablated wing disc. The open arrowhead

729 indicates weak TUNEL staining in the *salm* domain, while the lateral TUNEL staining is

730 no longer observed in the presence of P35.

731 (**I-J**) Regeneration scoring of adult wings from early and late L3 discs ablated by *DC^{rpr}*

732 (**I**) or *DC^{GluR1}* (**J**) in the presence and absence of P35. Number of wings scored: early

733 and late L3 *DC^{rpr}* (n = 74, n = 87), early and late L3 *DC^{rpr}>>p35* (n = 110, n = 125), early

734 and late L3 *DC^{GluRI}* (n = 100, n = 38), early and late L3 *DC^{GluRI}>>p35* (n = 101, n = 27).

735 (**K-L'**) Adult wing phenotypes following ablation with *DC^{rpr}* (**K**) or *DC^{rpr}>>p35* (**K'**), and

736 *DC^{GluR1}* (**L**) and *DC^{GluR1}>>p35* (**L'**). Arrowheads indicate an incomplete L5 vein, which is

737 a consequence of *p35* expression on vein development, reported previously (Perez-

738 Garijo et al. 2004).

739 (**M**) The mean area of adult wings from discs ablated with *DC*^{rpr} (n = 31), *DC*^{rpr}*>>p35* (n

740 = 19), *DC*^{GluR1} (n = 10), and *DC*^{GluR1}*>>p35* (n = 15), ns, not significant, *** p = 0.0002,

741 data analyzed by one-factor ANOVA and Tukey's multiple comparisons test.

Figure 4

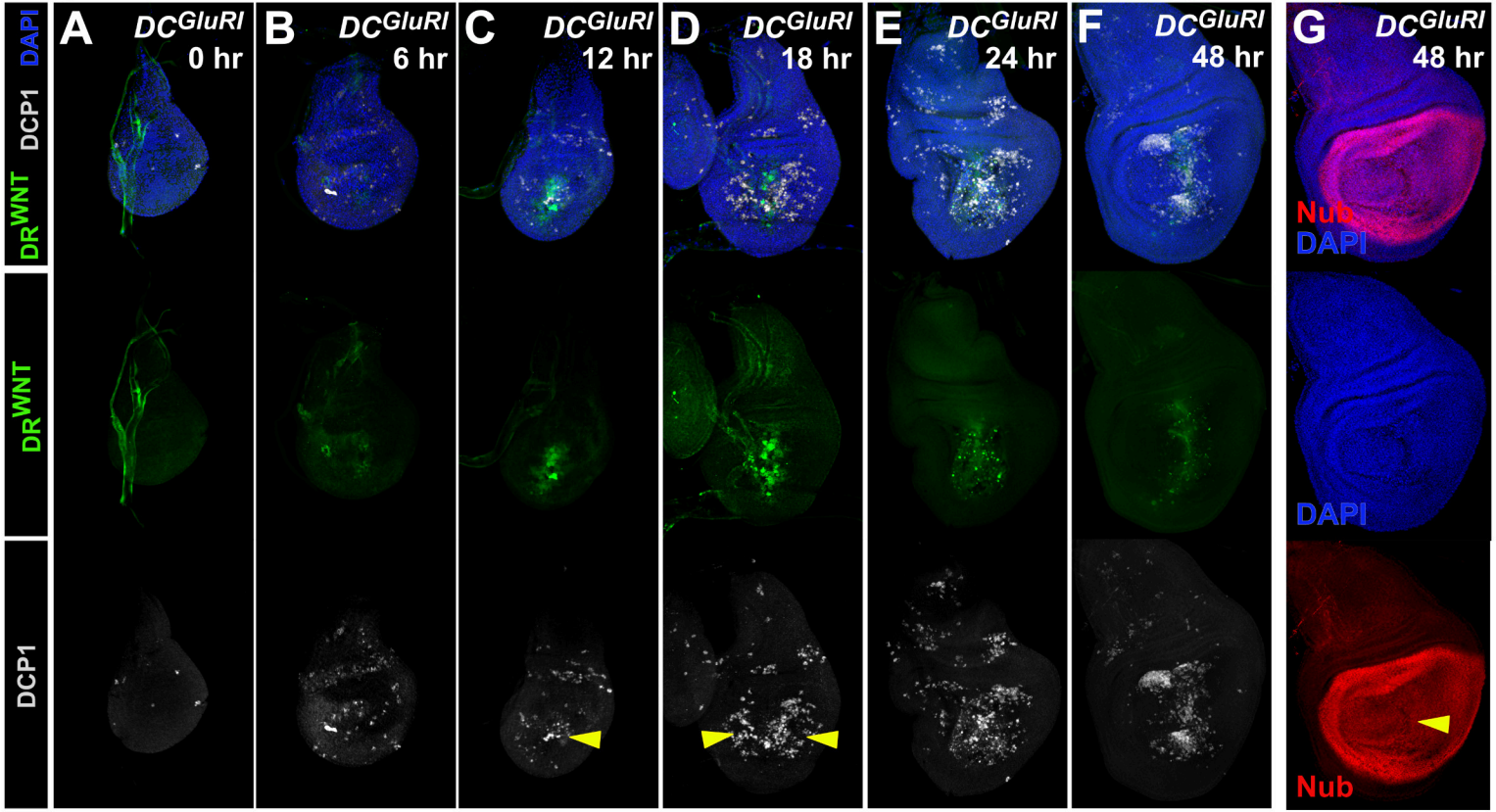
A
DCGluRI
0 hr
B
DCGluRI
6 hr
C
DCGluRI
12 hr
D
DCGluRI
18 hr
E
DCGluRI
24 hr
F
DCGluRI
48 hr
G
DCGluRI
48 hr
DRWNT
DCP1
DAPI
Nub

742 **Figure 4. Necrosis-induced apoptosis (NiA) forms after wound edge signaling**
743 **occurs.**
744 (**A-F**) A time course of regeneration for wing discs bearing a fluorescent reporter of a
745 damage-responsive WNT enhancer (DR^{WNT}, green, (Harris et al. 2016) ablated with
746 DC^{GluR1} and stained for DCP1 (gray) at (**A**) 0 hr, (**B**) 6 hr, (**C**) 12 hr, (**D**) 18 hr, (**E**) 24 hr,
747 (**F**) 48 hr after heat shock. Arrowhead in (C) indicates wound edge apoptosis at 6 hr
748 coinciding with the appearance of DR^{WNT} expression, arrowheads in (D) indicates NiA at
749 18 hr.
750 (**G**) A wing imaginal disc at 48 hr of recovery following ablation with DC^{GluR1}. The pouch
751 marker Nub (red) and DAPI staining (blue) show continuity of the pouch is restored
752 (arrowhead).

Figure 5

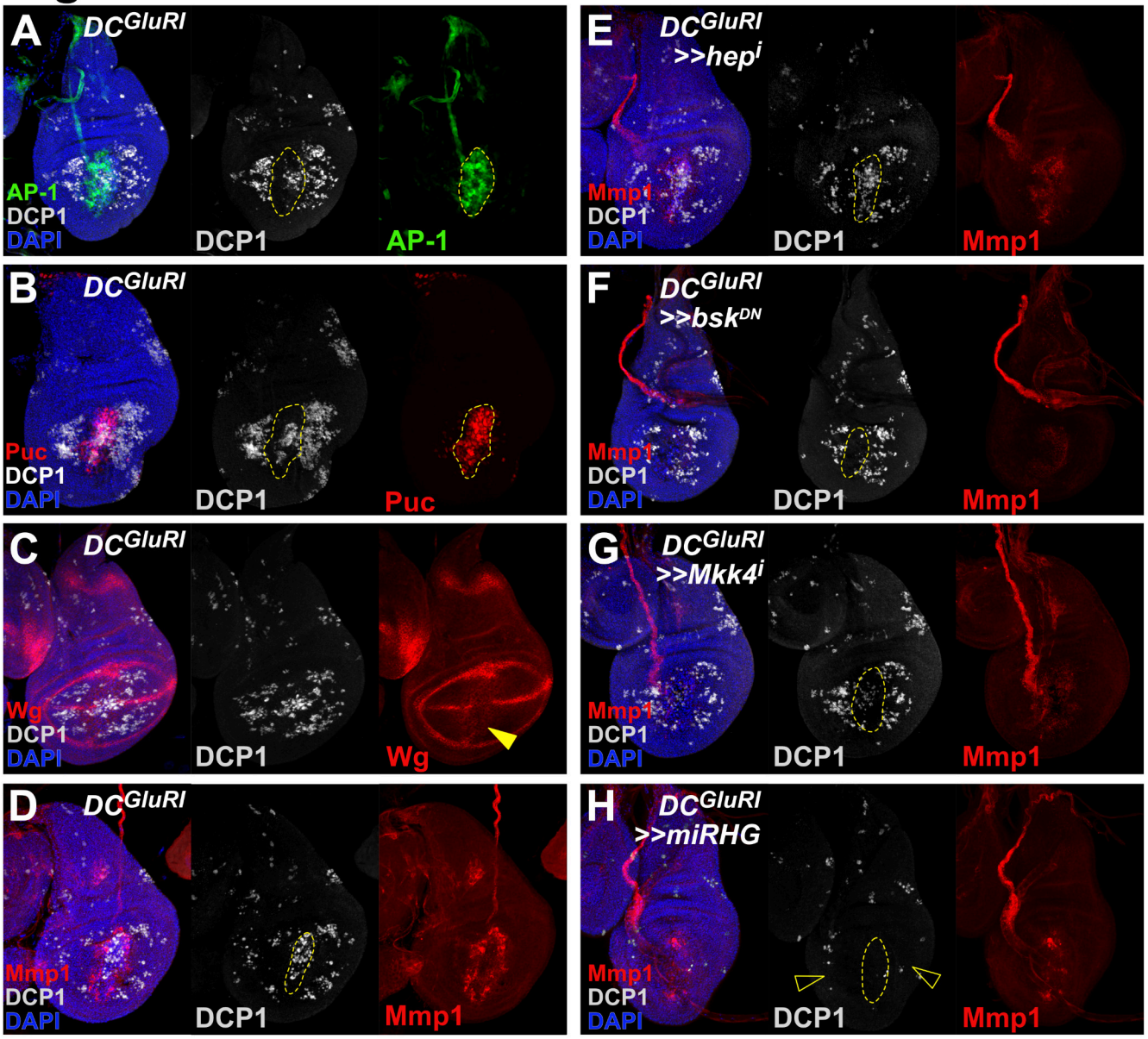
A
DC^GluRI
AP-1
DCP1
DAPI
DCP1
AP-1
B
DC^GluRI
Puc
DCP1
DAPI
DCP1
Puc
C
DC^GluRI
Wg
DCP1
DAPI
DCP1
Wg
D
DC^GluRI
Mmp1
DCP1
DAPI
DCP1
Mmp1
E
DC^GluRI
>>hep^i
Mmp1
DCP1
DAPI
DCP1
Mmp1
F
DC^GluRI
>>bsk^DN
Mmp1
DCP1
DAPI
DCP1
Mmp1
G
DC^GluRI
>>Mkk4^i
Mmp1
DCP1
DAPI
DCP1
Mmp1
H
DC^GluRI
>>miRHG
Mmp1
DCP1
DAPI
DCP1
Mmp1

753 **Figure 5. Necrosis-induced apoptosis (NiA) acts independently of the JNK**
754 **pathway.**
755 (**A-B**) Wing discs ablated with *DC*^{GluR1} and bearing the *AP-1-GFP* (green) (**A**) and
756 *puc*^{A251} (red) (**B**) reporters of JNK pathway activity and stained for DCP1 (gray), DAPI,
757 blue. These reporters show strong overlap with the wound edge apoptosis, but not with
758 the NiA cells. As in other panels, the dashed line outlines the ablated *salm* domain,
759 indicated by the appearance of cells labelled by DAPI.
760 (**C-D**) Wing imaginal discs ablated with *DC*^{GluR1} and stained for the JNK targets Wg
761 (red) (**C**) and Mmp1 (red) (**D**). DCP1, gray; DAPI, blue. Arrowhead in (C) indicates
762 ectopic Wg at the wound edge.
763 (**E**) A wing imaginal disc ablated with *DC*^{GluR1}*>>hep*^{RNAi} stained for DCP1 (gray) and
764 Mmp1 (red), DAPI, blue. Both the wound edge apoptosis and NiA cells remain
765 unaffected following knockdown of *hep*.
766 (**F**) A wing imaginal disc ablated with *DC*^{GluR1}*>>bsk*^{DN} stained for DCP1 (gray) and
767 Mmp1 (red), DAPI, blue. Wound edge apoptosis is largely absent, while NiA cells
768 remain unaffected.
769 (**G**) A wing imaginal disc ablated with *DC*^{GluR1}*>>Mkk4*^{RNAi} stained for DCP1 (gray) and
770 Mmp1 (red), DAPI, blue. Wound edge apoptosis is strongly reduced, while NiA cells
771 remain unaffected.
772 (**H**) A wing imaginal disc ablated with *DC*^{GluR1}*>>miRHG* stained for DCP1 (gray) and
773 Mmp1 (red), DAPI, blue. Both the wound edge apoptosis and NiA (open arrowheads)
774 are eliminated following knockdown of *rpr, hid,* and *grim* with *miRHG*.

Figure 6

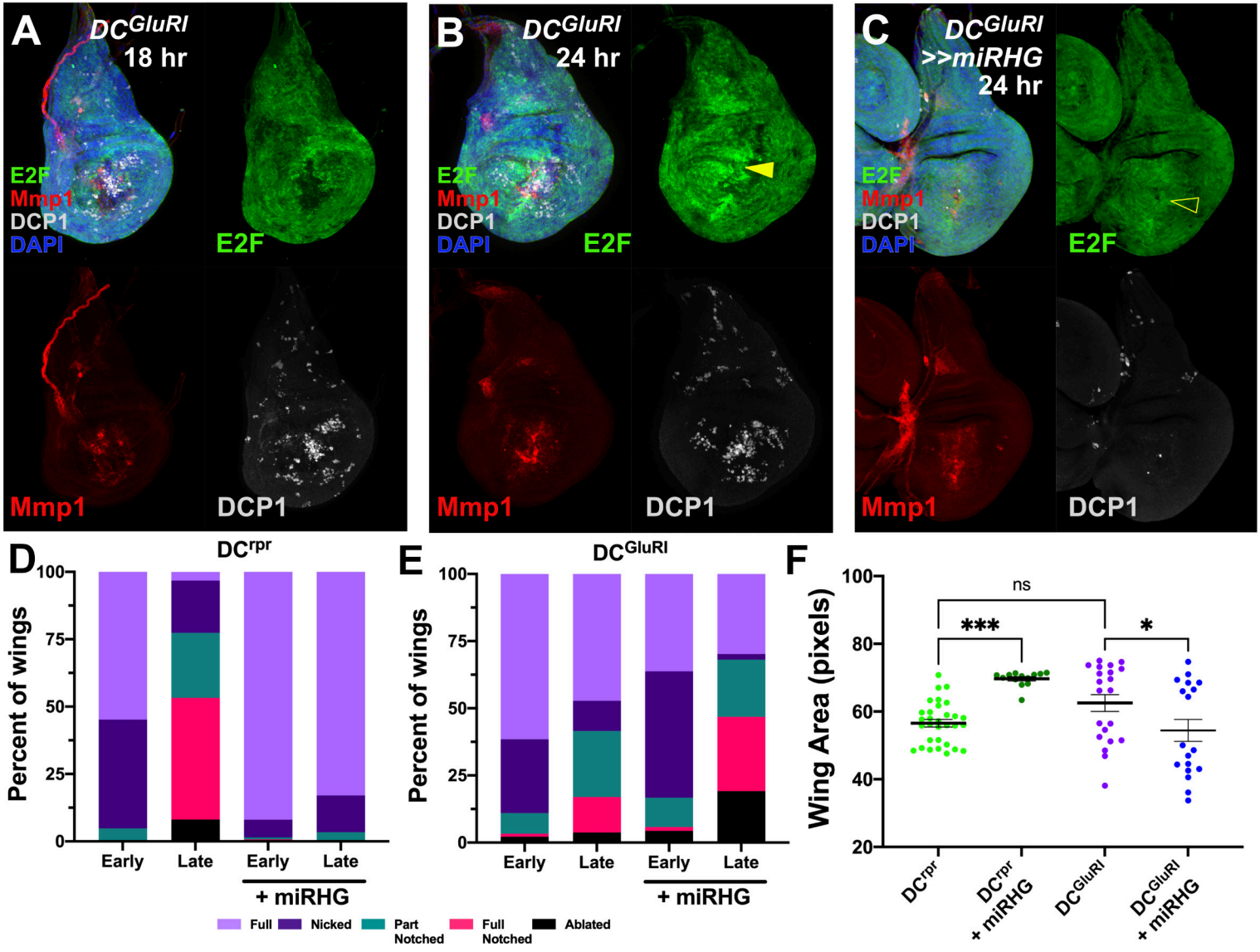
A
DCGluRI
18 hr
E2F
Mmp1
DCP1
DAPI
E2F
Mmp1
DCP1
B
DCGluRI
24 hr
E2F
Mmp1
DCP1
DAPI
E2F
Mmp1
DCP1
C
DCGluRI
>>miRHG
24 hr
E2F
Mmp1
DCP1
DAPI
E2F
Mmp1
DCP1
D
DCrpr
Percent of wings
100
75
50
25
0
Early
Late
Early
Late
+ miRHG
E
DCGluRI
Percent of wings
100
75
50
25
0
Early
Late
Early
Late
+ miRHG
Full
Nicked
Part Notched
Full Notched
Ablated
F
Wing Area (pixels)
100
80
60
40
20
ns
***
*
DCrpr
DCrpr + miRHG
DCGluRI
DCGluRI + miRHG

775 **Figure 6. Blocking NiA cell activity impairs regeneration.**

776 (**A-B**) Wing discs bearing an *E2F* transcriptional reporter (*PCNA-GFP,* green) ablated
777 with DC^{GluR1} and stained for Mmp1 (red) and DCP1 (gray) at 18 hr (**A**) and 24 hr (**B**) of
778 recovery. DAPI, blue. Arrowhead in (B) shows the regeneration blastema that is only
779 present after 24 hr of recovery.

780 (**C**) Wing disc bearing *PCNA-GFP* (green) ablated with A DC^{GluR1}*>>miRHG* and stained
781 for Mmp1 (red) and DCP1 (gray), DAPI, blue. The open arrowhead indicates a reduced
782 proliferation upon *miRHG* expression. JNK signaling, indicated by Mmp1 staining, is still
783 present in these discs.

784 (**D-E**) Regeneration scoring of adult wings from early and late L3 discs ablated with
785 DC^{rpr} (**D**) or DC^{GluR1} (**E**) in the presence and absence of *miRHG*. Number of wings
786 scored: early and late L3 DC^{rpr} (n = 62, n = 63), early and late L3 DC^{rpr}*>>miRHG* (n =
787 137, n = 88), early and late L3 DC^{GluRI} (n = 91, n = 53), early and late L3
788 DC^{GluRr}*>>miRHG* (n = 138, n = 47). While *miRHG* leads to more full and nicked wings
789 following DC^{rpr} ablation, the opposite is seen following DC^{GluR1} ablation.

790 (**F**) Mean pixel area of adult wings from late L3 discs ablated with DC^{rpr} (n = 31),
791 DC^{rpr}*>>miRHG* (n = 13), DC^{GluR1} (n = 21) and DC^{GluR1}*>>miRHG* (n = 18). ns: not
792 significant, * $p < 0.0439$, *** $p = 0.0004$, data analyzed by one-factor ANOVA and
793 Tukey's multiple comparisons tests**.**

Figure 7

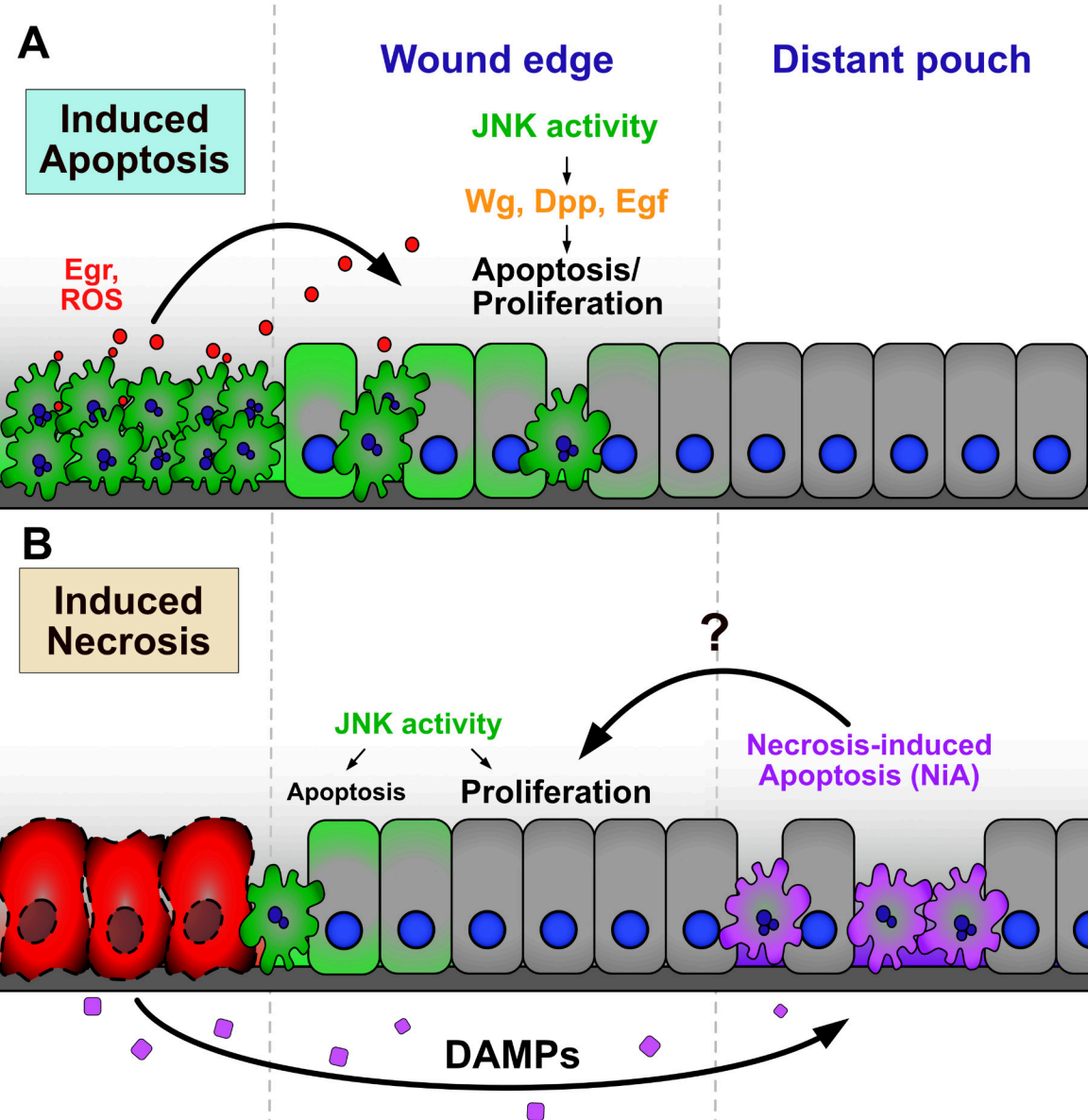
A
Wound edge
Distant pouch
Induced Apoptosis
JNK activity
Wg, Dpp, Egf
Apoptosis/ Proliferation
Egr, ROS
B
Induced Necrosis
?
JNK activity
Apoptosis
Proliferation
Necrosis-induced Apoptosis (NiA)
DAMPs

794 **Figure 7. NiA cells promotes regeneration in *DC^{GluR1}* ablated discs**

795 (**A-B**) Schematics depicting the cell signaling events that occur resulting from apoptotic
796 ablation with *DC^{hepCA}* (**A**) and necrotic ablation with *DC^{GluRI}* (**B**). Dying cells release
797 reactive oxygen species (ROS) and promote Egr release via hemocytes and potentially
798 other mechanisms, inducing high levels of JNK signaling at the wound edge. In turn,
799 wound edge apoptotic cells and surviving cells with lower JNK signaling release
800 mitogens including Wg, Dpp, and Egf, to promote regenerative signaling in the adjacent
801 wound edge tissue. In cells undergoing necrosis, low levels of ligand-independent JNK
802 signaling occurs at the wound edge, likely through pathways related to polarity
803 disruption, mechanical stress or immediate stress signals such as ROS. This signaling
804 induces sporadic apoptosis at the wound edge that potentially contributes to
805 proliferation and recovery. Necrotic cells also release an as yet unidentified long-range
806 signal that could be a damage associated molecular pattern (DAMP), resulting in the
807 formation of NiA cells in the distant pouch. These cells promote proliferative blastema
808 formation and regeneration.

Figure S1

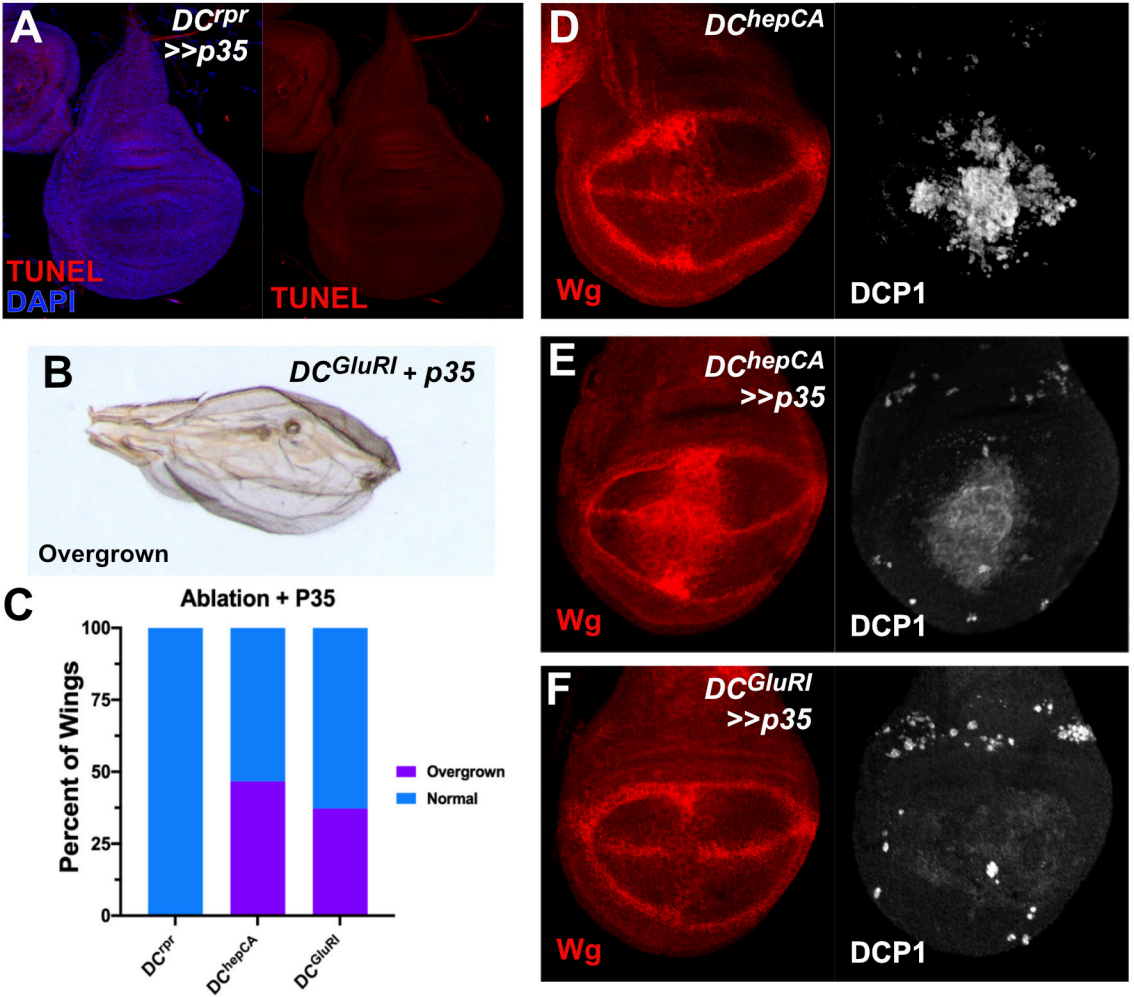
A
DCrpr
>>p35
TUNEL
DAPI
TUNEL
B
DCGluRI + p35
Overgrown
C
Ablation + P35
Percent of Wings
100
75
50
25
0
Overgrown
Normal
DCrpr
DChepCA
DCGluRI
D
DChepCA
Wg
DCP1
E
DChepCA
>>p35
Wg
DCP1
F
DCGluRI
>>p35
Wg
DCP1

Supplemental Figure Legends

Figure S1. Related to Figure 3

Blocking apoptosis with P35 leads to wing overgrowth phenotypes

(**A**) A wing disc labelled with a TUNEL (red) following *DC^{rpr}>>p35* ablation. DAPI, blue. The lack of signal demonstrates the ability of P35 to inhibit cell death.

(**B**) Adult wing showing the overgrown phenotype accompanied by blistering and ectopic vein tissue observed following *DC^{GluR1}>>p35* ablation.

(**C**) A graph representing the frequency of overgrown wings following ablation with *DC^{rpr}>>p35*, *DC^{hepCA}>>p35* and *DC^{GluR1}>>p35*. No overgrown wings were observed in *DC^{rpr}>>p35*.

(**D-F**) Wing imaginal discs stained for Wg (red) and DCP1 (gray) following ablation by *DC^{hepCA}* (**D**), *DC^{hepCA}>>p35* (**E**) or *DC^{GluR1}>>p35* (**F**). Ectopic Wg overlaps with the diffuse DCP1 signal in *DC^{hepCA}>>p35*, discs however, little Wg is associated with the blocked apoptotic cells of *DC^{GluR1}>>p35* discs.

Figure S2

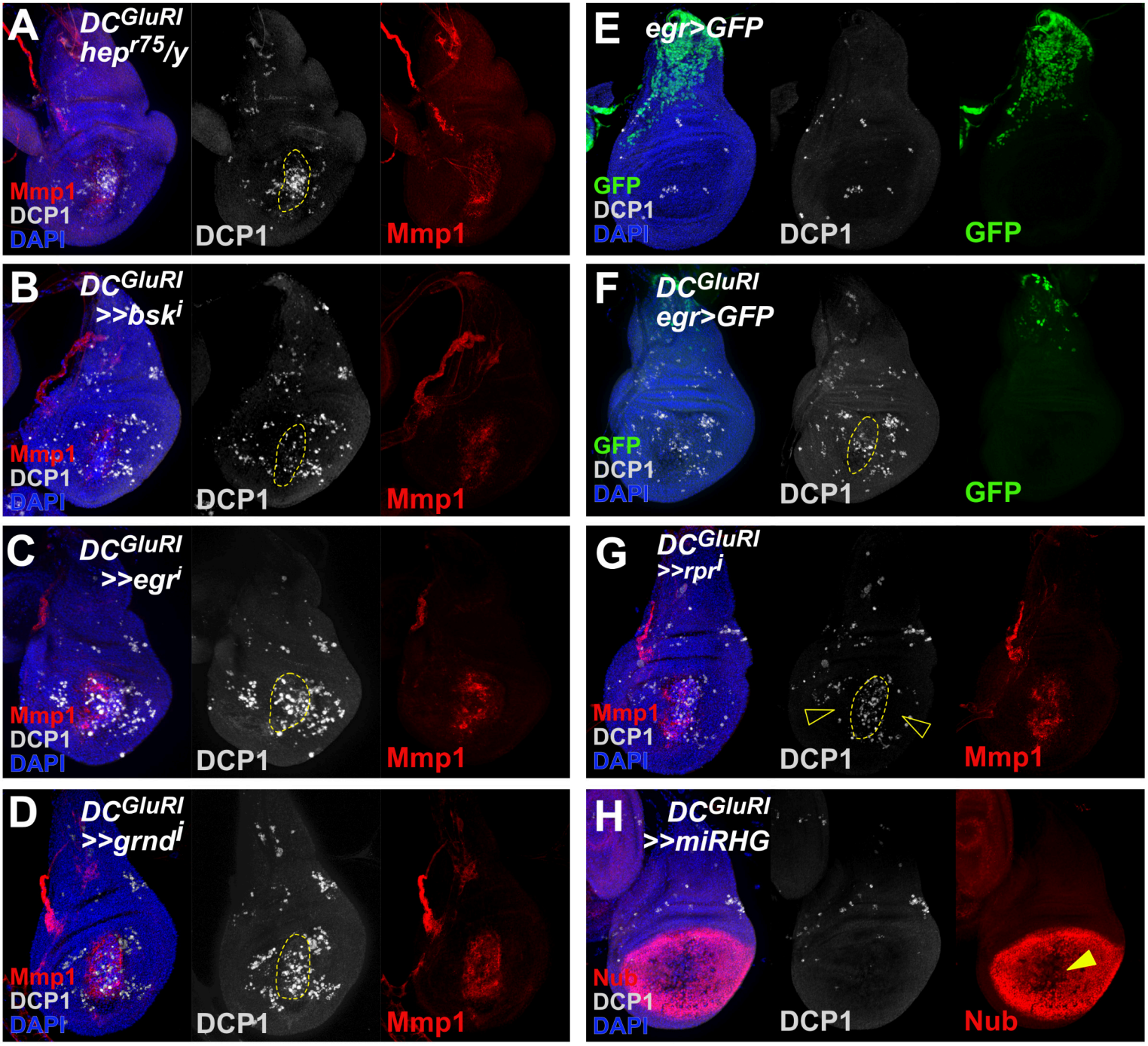
A
DC^GluRI
hep^r75/y
Mmp1
DCP1
DAPI
DCP1
Mmp1
B
DC^GluRI
>>bsk^i
Mmp1
DCP1
DAPI
DCP1
Mmp1
C
DC^GluRI
>>egr^i
Mmp1
DCP1
DAPI
DCP1
Mmp1
D
DC^GluRI
>>grnd^i
Mmp1
DCP1
DAPI
DCP1
Mmp1
E
egr>GFP
GFP
DCP1
DAPI
DCP1
GFP
F
DC^GluRI
egr>GFP
GFP
DCP1
DAPI
DCP1
GFP
G
DC^GluRI
>>rpr^i
Mmp1
DCP1
DAPI
DCP1
Mmp1
H
DC^GluRI
>>miRHG
Nub
DCP1
DAPI
DCP1
Nub

Figure S2. Related to Figure 5.

Manipulation of JNK pathway elements in *DC^{GluRI}* ablated discs.

(**A**) A wing imaginal disc stained for DCP1 (gray) and Mmp1 (red) following *DC^{GluR1}* ablation in a *hep^{r75}* hemizygous background. Wound edge apoptosis and NiA cells are still observed in this background, although are overall reduced. DAPI, blue. As in other panels, the dashed line outlines the ablated *salm* domain, indicated by the change in DAPI appearance.

(**B**) A wing imaginal disc stained for DCP1 (gray) and Mmp1 (red) following *DC^{GluR1}>>bsk^{RNAi}* ablation. DAPI, blue. Wound edge apoptotic cells are largely absent following *bsk* knockdown, while NiA cells remain unaffected,.

(**C**) A wing imaginal disc stained for DCP1 (gray) and Mmp1 (red) following *DC^{GluR1}>>egr^{RNAi}* ablation. DAPI, blue. Both wound edge apoptotic cells and NiA cells remain unaffected by *egr* knockdown.

(**D**) A wing imaginal disc stained for DCP1 (gray) and Mmp1 (red) following *DC^{GluR1}>>grnd^{RNAi}* ablation. DAPI, blue. As in (C), both wound edge apoptotic cells and NiA cells remain unaffected following *grnd* knockdown.

(**E-F**) Discs bearing an *egr* reporter (*egr-Gal4; UAS-GFP*, green) in an undamaged disc (**D**) and following ablation by *DC^{GluR1}* (**E**). Reporter activity is not observed in the pouch with or without ablation, but is seen in the notum.

(**G**) A wing imaginal disc stained for DCP1 (gray) and Mmp1 (red) following *DC^{GluR1}>>rpr^{RNAi}* ablation. DAPI, blue. Knockdown of *rpr* leads to a mild reduction of both wound edge apoptotic cells and NiA cells (open arrowheads).

(**H**) A wing imaginal disc stained for DCP1 (gray) and Nub (red) following *DC*^{GluR1}*>>miRHG* ablation. Tissue loss indicated by loss of Nub (arrowhead) is still observed following ablation with *DC*^{GluR1} despite apoptosis inhibition by knockdown of *rpr, hid,* and *grim.*

Figure S3

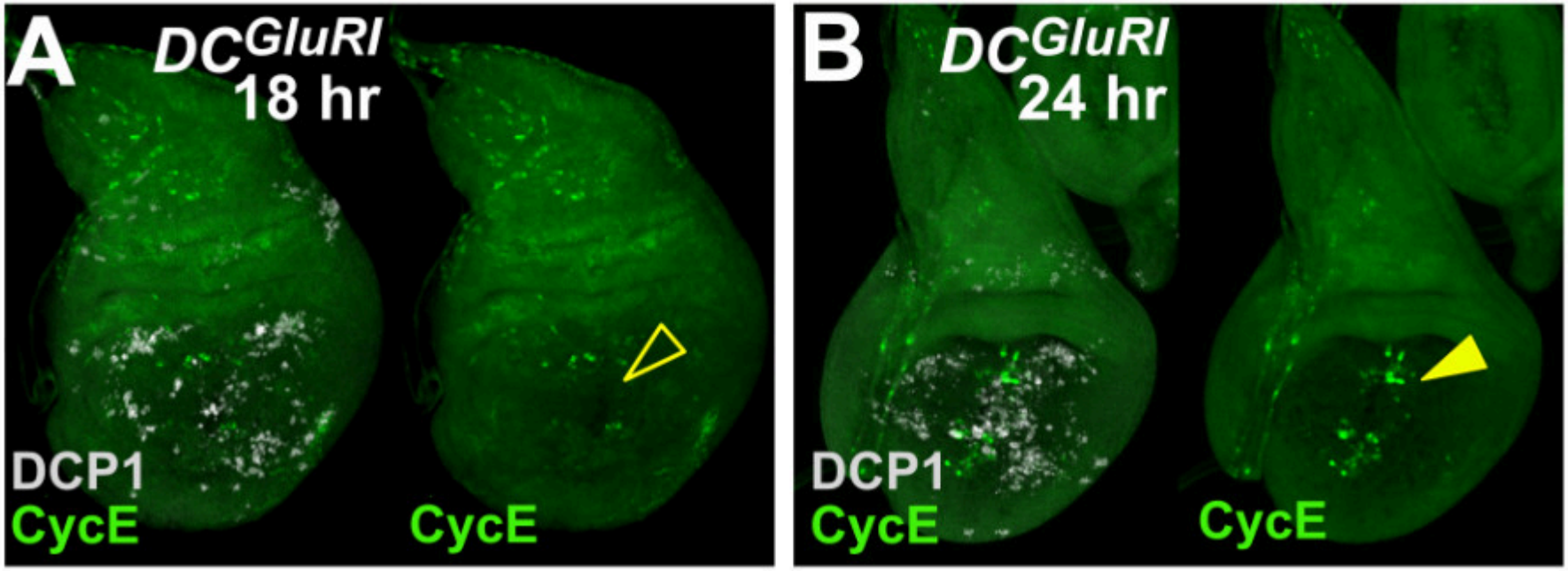

Figure S3. Related to Figure 6.

(**A-B)** Wing imaginal discs bearing the *CycE-GFP* reporter (green) at 18 hr (**A**) and 24 hr (**B**) of recovery following ablation by DC^{GluR1}. The open arrowhead in (A) indicates a lack of reporter activity in the *salm* domain, while the arrowhead in (B) highlights stronger reporter activity at 24 hr.